SOME CONSIDERATIONS ON PREVENTION OF CHATTER VIBRATION IN MULTI-EDGE ROTARY CUTTING TOOLS

SHINOBU KATO and ETSUO MARUI

Department of Mechanical Engineering

(Received September 26, 1969)

CONTENTS

1. Introduction

The cutting of metals is frequently accompanied by vibrations of cutting tool or workpiece, known as "chatter vibration". The existence of chatter vibration is a serious problem because it is detrimental to the life of tool, to the surface finish and to the accuracy of the machined parts. Though an elucidation of the problem is very important in these respects, the radical improvement of the chatter behaviour is extremely difficult because chatter vibration is of a very complex nature. In recent years, however, many workers have become to study on chatter vibrations, and useful results are obtained[1)~4)]. Especially the general analytical method of chatter vibration which is shown by Merrit *et al.*[5)] is rated high. Nevertheless, detailed experiments and investigations are necessary to prevent the chatter vibration in each cutting operation.

In boring operation, high finish and accuracy are generally required. It is also desired to raise the length-diameter ratio of the hole to be bored. However, owing to the insufficient rigidity of boring bars, chatter vibration is liable to occur in boring operations. Many procedures have been used to prevnt the chatter vibration and to obtain a high degree of precision, and obtained fairly good results. For example, Hahn[6)] showed that the chatter vibration of boring bar can effectively be prevented by the Lanchester Damper, and Kato *et al.*[7)] suggested the way to design the optimum damper. Furthermore, Kuchma[8)] suggested that the chatter vibration of boring bars can be prevented, and the efficiency of the operation is raised by using the directional characteristics in the vibrational properties of the boring bar.

It may usually be inevitable that the boring bar has a directional characteristics in the vibrational properties (that is, stiffness, natural frequency, damping coefficient), owing to the mechanisms of the transmission of torque or tool holding devices. In this paper, first, the relationship between the stability boundary of chatter and the vibrational properties, the cutting conditions, is obtained theoretically for the boring bars which have directional characteristics in the vibrational properties, and on the basis of this result, the optiumum configuration of boring bar and the optimum setting condition of a tool to the boring bar to prevent the chatter are discussed.

It may be inevitable that the multi-edge rotary cutting tools such as drill, tap and reamer have a directional characteristics in the vibrational propeties, owing to the structure of the tools, too. Then, the stability boundary of chatter is introduced theoretically as the function of the vibrational properties of the system and the various cutting conditions, using the same method as the analysis of the boring bar, and is ascertained experimentally. And on the basis of this, the concrete means for the prevention of the chatter in the multi-edge rotary cutting tool are examined in detail.

Furthermore, the effect of a small error in the tool setting condition and in the tool dimensions (such as cutting angle, nose radius etc.) is studied for many practical cases.

2. Some Considerations on the Prevention of Chatter Vibration in Boring Operation[9)10)]

2.1. Analysis

2.1.1. Equation of motion and stability boundary

First, the differential equation representing the chatter vibration occuring in boring bars with directional characteristics in their vibrational properties as shown in Fig. 1 will be determined, and the stability boundary of chatter will be discussed theoretically.

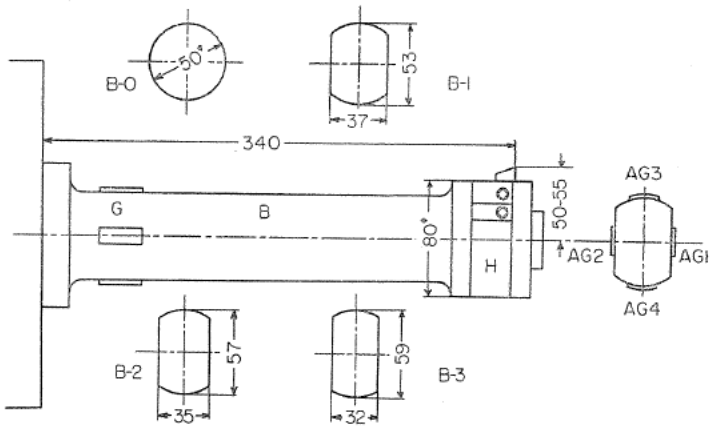

FIG. 1. Diagram of boring bars.

For the sake of simplicity, the boring bars are regarded as a lumped mass system with two degrees of freedom, and following is a treatment of chatter vibration occuring in orthogonal cutting operations. The analytical results, however, include other cutting operations.

In Fig. 2, center A of the boring bar displaces to point O under the action of the cutting force in a cutting operation. Taking this point O as the origin, x-axis is determined in the direction of the least stiffness of the boring bar, and y-axis in the direction of the greatest. This coordinate system rotates with the same velocity as a boring bar. When the cutting operation is steady, the boring bar displaces to the amount of a_x along the x-axis and a_y along the y-axis by the cutting force respectively. If the corresponding depth of cut is denoted by d_s, then

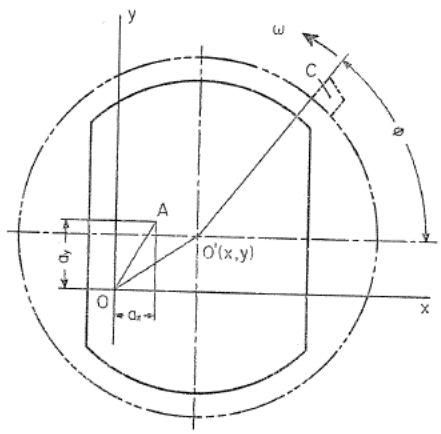

FIG. 2. Rotational coordinate system fixed to boring bar.

$$\left.\begin{aligned} -F_{sx}(d_s) &= (k_x - m\omega^2)a_x \\ -F_{sy}(d_s) &= (k_y - m\omega^2)a_y \end{aligned}\right\} \quad (1)$$

where $F_{sx}(d_s)$, $F_{sy}(d_s)$ represent the components of the cutting force in the x and y directions, $k_x a_x$, $k_y a_y$ are the spring forces in both directions, and $-m\omega^2 a_x$, $-m\omega^2 a_y$ are the centrifugal forces respectively.

Representing the angle between the x-axis and the cutting edge setting direction by ϕ, the depth of cut during vibration can be expressed as follows:

$$d = d_s + (x\cos\phi + y\sin\phi) \tag{2}$$

According to Doi and the author's previous investigations, the occurence of the chatter seems to be caused by the time lag of the cutting force existing behind the fluctuations in area of the cut[4]. On the basis of this investigation, and assuming that the components of the cutting force are proportional to the depth of cut, the thrust force F_N and the cutting force F_T can be written as follows:

$$\left.\begin{aligned} F_N &= K_N\{d_s + x(t-H)\cos\phi + y(t-H)\sin\phi\} \\ F_T &= K_T\{d_s + x(t-h)\cos\phi + y(t-h)\sin\phi\} \end{aligned}\right\} \tag{3}$$

where H and h indicate time lags of thrust and cutting force respectively, and K_T and K_N are the proportional coefficients of the cutting and the thrust force respectively. Hence, K_T, K_N are closely related to the cutting conditions (that is, material being cut, geometry of cutting tool, width of cut and so on).

The x and y components of the cutting force, that is, F_x and F_y, can be written as functions of F_N, F_T as follows:

$$\left.\begin{aligned} F_x &= F_N\cos\phi - F_T\sin\phi \\ F_y &= F_N\sin\phi + F_T\cos\phi \end{aligned}\right\} \tag{4}$$

For the sake of simplisity, the following notations are used.

$$\left.\begin{aligned} x(t-H) &= x_{(H)},\ y(t-H) = y_{(H)} \\ x(t-h) &= x_{(h)},\ y(t-h) = y_{(h)} \end{aligned}\right\} \tag{5}$$

Substituting Eqs. (3) and (5) in Eq. (4), the expression for F_x, F_y is given.

$$\left.\begin{aligned} F_x &= F_{sx}(d_s) + K_N x_{(H)}\cos^2\phi + (K_N y_{(H)} - K_T x_{(h)})\sin\phi\cos\phi - K_T y_{(h)}\sin^2\phi \\ F_y &= F_{sy}(d_s) + K_T x_{(h)}\cos^2\phi + (K_N x_{(H)} + K_T y_{(h)})\sin\phi\cos\phi + K_N y_{(H)}\sin^2\phi \end{aligned}\right\} \tag{6}$$

where

$$\left.\begin{aligned} F_{sx}(d_s) &= K_N d_s\cos\phi - K_T d_s\sin\phi \\ F_{sy}(d_s) &= K_N d_s\sin\phi + K_T d_s\cos\phi \end{aligned}\right\} \tag{7}$$

Using the above equations, the differential equation representing chatter vibration can be derived in the rotational coordinate system. Here, it may be allowed to neglect the coupling effect induced from gyromoment, since the equivalent mass of the boring bar and the polar moment of inertia about the axis of rotation are generally small. Therefore, the centrifugal force and Corioli's force have only been taken into consideration, and the differential equation of chatter vibration becomes,

$$\left.\begin{aligned} &m\ddot{x} + c_x\dot{x} + (k_x - m\omega^2)(x + a_x) - 2m\omega\dot{y} + F_x = 0 \\ &2m\omega\dot{x} + m\ddot{y} + c_y\dot{y} + (k_y - m\omega^2)(y + a_y) + F_y = 0 \end{aligned}\right\} \tag{8}$$

where m is the equivalent mass of the boring bar and it is assumed that the values of m in x and y directions are equal referring to the experimental results given later. c_x, c_y are the damping coefficients and k_x, k_y are the spring constants in both directions respectively. ω is the angular velocity of the boring bar.

Setting

$$c_x/m=2n_x,\ c_y/m=2n_y,\ k_x/m=p_x^2,\ k_y/m=p_y^2,\ K_N/m=\lambda_N,\ K_T/m=\lambda_T \tag{9}$$

It is justifiable that the time lags H, h of the cutting force are such small amounts that $x_{(H)}$, $y_{(H)}$, etc. are approximated as follows:

$$\left.\begin{aligned} x_{(H)}&=x-H\dot{x},\ y_{(H)}=y-H\dot{y}\\ x_{(h)}&=x-h\dot{x},\ y_{(h)}=y-h\dot{y}\end{aligned}\right\} \tag{10}$$

Using Eqs. (1), (6), (7), (9) and (10), Eq. (8) becomes,

$$\left.\begin{aligned} &\ddot{x}+(2n_x-\lambda_N H\cos^2\phi+\lambda_T h\sin\phi\cos\phi)\dot{x}+(p_x^2-\omega^2+\lambda_N\cos^2\phi-\lambda_T\sin\phi\cos\phi)x\\ &\quad+(-2\omega-\lambda_N H\sin\phi\cos\phi+\lambda_T h\sin^2\phi)\dot{y}+(\lambda_N\sin\phi\cos\phi-\lambda_T\sin^2\phi)=0\\ &(2\omega-\lambda_N H\sin\phi\cos\phi-\lambda_T h\cos^2\phi)\dot{x}+(\lambda_N\sin\phi\cos\phi+\lambda_T\cos^2\phi)x+\ddot{y}\\ &\quad+(2n_y-\lambda_N H\sin^2\phi-\lambda_T h\sin\phi\cos\phi)\dot{y}+(p_y^2-\omega^2+\lambda_N\sin^2\phi\\ &\qquad+\lambda_T\sin\phi\cos\phi)y=0\end{aligned}\right\} \tag{11}$$

For the convenience of numerical calculations, the following non-dimensional expressions are used.

$$\left.\begin{aligned} &t_0=p_x t,\ \xi=x/a_x,\ d\xi/dt_0=\dot{x}/a_x p_x,\ \ldots,\\ &r=p_y/p_x,\ n_0=2n_x/p_x,\ q=n_y/n_x,\ \omega_0=\omega/p_x,\\ &H_0=p_x H,\ \lambda_0=\lambda_N/p_x^2,\ \varepsilon=h/H,\ \tau=\lambda_T/\lambda_N\end{aligned}\right\} \tag{12}$$

where ε indicates the ratio of time lags in the cutting force, and τ indicates the ratio of K_T to K_N, namely, of the two components of the cutting force (See Eqs. (3) and (9)).

Eliminating the terms including y from Eq. (11) and using the non-dimensional expressions of (12), it follows,

$$d^4\xi/dt_0^4+Td^3\xi/dt_0^3+Ud^2\xi/dt_0^2+Vd\xi/dt_0+W=0 \tag{13}$$

$$\left.\begin{aligned} T&=n_0(1+q)-\lambda_0 H_0\\ U&=1+r^2+2\omega_0^2+qn_0+\lambda_0\{1-2\tau\varepsilon H_0\omega_0-(\sin^2\phi+q\cos^2\phi)n_0 H_0\\ &\quad-\tau\varepsilon H_0 n_0(1-q)\sin\phi\cos\phi\}\\ V&=n_0\{q+r^2-(1+q)\omega_0^2\}+\lambda_0[\omega_0^2 H_0+2\tau\omega_0-(H_0-n_0)\sin^2\phi\\ &\quad-\{\tau n_0(q-1)+\tau\varepsilon H_0(1-r^2)\}\sin\phi\cos\phi-(r^2 H_0-qn_0)\cos^2\phi]\\ W&=r^2-(1+r^2-\omega_0^2)\omega_0^2+\lambda_0\{-\omega_0^2+\sin^2\phi-(r^2-1)\tau\sin\phi\cos\phi+r^2\cos^2\phi\}\end{aligned}\right\} \tag{14}$$

Now, assuming the solution of Eq. (13) is as follows:

$$\xi = \xi_0 e^{zt} \tag{15}$$

and substituting (15) in (13), Eq. (13) becomes

$$z^4 + Tz^3 + Uz^2 + Vz + W = 0 \tag{16}$$

The roots of Eq. (16) can be written in the form of a complex number.

$$\left.\begin{aligned} &z_{1,2} = \alpha_1 \pm j\beta_1, \quad z_{3,4} = \alpha_2 \pm j\beta_2 \\ &\text{where } j = \sqrt{-1} \end{aligned}\right\} \tag{17}$$

Using the relations mentioned above, it follows,

$$\left.\begin{aligned} T &= -2(\alpha_1 + \alpha_2) \\ U &= \alpha_1^2 + \alpha_2^2 + \beta_1^2 + \beta_2^2 + 4\alpha_1\alpha_2 \\ V &= -2\alpha_1(\alpha_2^2 + \beta_2^2) - 2\alpha_2(\alpha_1^2 + \beta_1^2) \\ W &= (\alpha_1^2 + \beta_1^2)(\alpha_2^2 + \beta_2^2) \end{aligned}\right\} \tag{18}$$

The necessary and sufficient condition that the solution given by Eqs. (15) and (17) is stable (that is, the system is stable for chatter vibration) is that the real parts of (17) are negative.

$$\alpha_{1,2} < 0 \tag{19}$$

At the stability boundary of chatter, the larger one of α_1, α_2 becomes zero. Hence, using this relation, and eliminating β_1, β_2 and α_1 or α_2, the following expression for the stability boundary of chatter vibration can be obtained.

$$TUV - V^2 - T^2 W = 0 \tag{20}$$

In Eqs. (20) and (14), parameters r, n, q, τ, ε and ϕ are determined by the vibrational properties or the cutting conditions. Hence, regarding these parameters as assigned, the critical value of λ_0 which gives the excitation boundary of chatter and frequency f corresponding to critical condition can be determined from Eq. (20) as follows:

$$\left.\begin{aligned} &(\lambda_0)_c = \lambda_0(r,\ n_0,\ q,\ \omega_0,\ H_0,\ \tau,\ \varepsilon,\ \phi) \\ &\text{or } (\lambda_N)_c = p_x^2 \cdot (\lambda_0)_c \\ &f = p_x / 2\pi \cdot \sqrt{V/T} \end{aligned}\right\} \tag{21}$$

Particularly, in the boring bars with no directional characteristics in vibrational properties, $r=1$, $q=1$. So that, Eq. (14) becomes

$$\left.\begin{aligned} T &= 2n_0 - \lambda_0 H_0 \\ U &= 2 + 2\omega_0^2 + n_0^2 + \lambda_0(1 - n_0 H_0 - 2\tau\varepsilon H_0\omega_0) \\ V &= 2n_0(1 + \omega_0^2) + \lambda_0(\omega_0^2 H_0 + 2\tau\omega_0 - H_0 + n_0) \\ W &= 1 - (2 - \omega_0^2)\omega_0^2 + \lambda_0(1 - \omega_0^2) \end{aligned}\right\} \tag{22}$$

In Eq. (22), it is a reasonable result that T, U, V and W do not include the

term of tool setting angle ϕ, and then the stability boundary of chatter in this case has no connection with ϕ.

2.1.2. Numerical calculation and consideration

Fig. 1 shows the dimensions of boring bars which are used in the following experiments and also in these numerical calculations.

The stiffness of a boring bar in both x and y directions (that is, k_x, k_y) is obtained from the load test, and the vibrational properties of boring bars (that is, natural frequencies p_x, p_y and damping coefficients n_x, n_y) are acquired from the free vibration photographs in Fig. 3. Using the above measurements of k, p, the equivalent mass m is given as follows:

$$m = k/p^2 \tag{23}$$

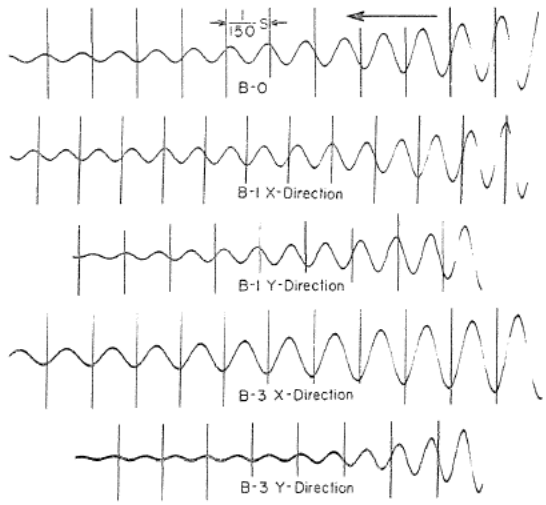

FIG. 3. Free vibrations of boring bars in x, y directions.

TABLE 1. Vibrational Properties of Boring Bars

	k_x (kg/mm)	k_y (kg/mm)	p_x (rad/s)	p_y (rad/s)	$\sqrt{(p_x^2+p_y^2)/2}$ (rad/s)	$r=p_y/p_x$	n_x (1/s)	n_y (1/s)	$(mg)_x$ (kg)	$(mg)_y$ (kg)
B-0	403		1223		1223	1	25.3		2.64	
B-1	323	507	1090	1373	1240	1.35	30.5	38.2	2.65	2.62
B-2	271	521	1009	1387	1212	1.40	22.1	40.1	2.62	2.66
B-3	249	560	954	1448	1227	1.52	20.1	57.7	2.67	2.63

These results are listed collectively in Table 1. From the table, it is obvious that, for every boring bar system, the equivalent mass m has an almost identical value in both x and y directions, and then the assumption made in the previous section is a reasonable one. It is also seen in the table that these four boring bars have an almost equal value of $\sqrt{(p_x^2+p_y^2)/2}$ or $(k_x+k_y)/2$.

As an example of this calculation, Figs. 4, 5 and 6 show the relations between the stability boundary $(\lambda_N)_c$ and the tool setting angle ϕ, which are obtained from Eqs. (20) and (14). Only the relationship within the range $0° \leqq \phi \leqq 180°$ is

illustrated in each figure, since there is a relationship that $(\lambda_N)_c(\phi) = (\lambda_N)_c(\phi+180°)$. In these calculations, the following numerical values are used referring to many previous experimental data, *i.e.*, $H=0.0005$ sec, $\varepsilon=0.4\sim0.8$, $\tau=2\sim4$. In these figures, any vibratory system becomes unstable in such a cutting condition that the individual value of λ_N is larger than that of $(\lambda_N)_c$ predicted by the corresponding $(\lambda_N)_c-\phi$ curve.

In the circular sectioned boring bar (that is, *B*-0), the stability boundary $(\lambda_N)_c$ is independent on the tool setting angle ϕ, seen as *B*-0 lines in Figs. 4, 5 and 6.

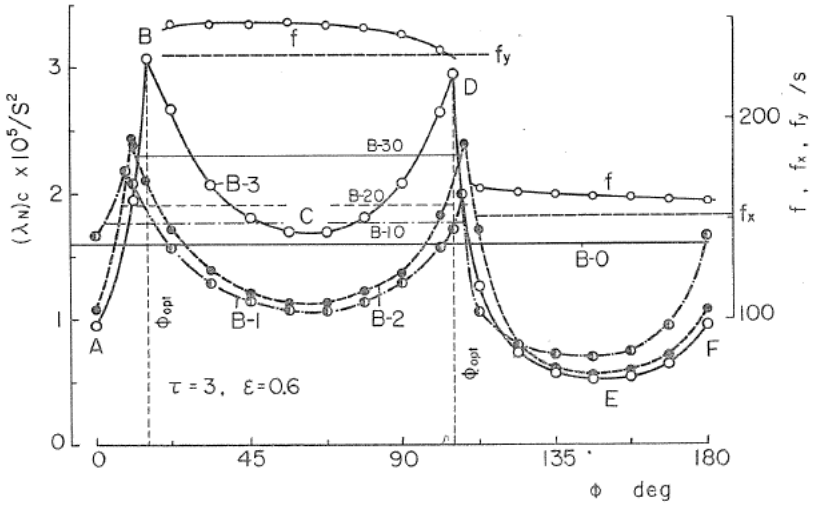

FIG. 4. Variation of stability boundary $(\lambda_N)_c$ and chatter frequency f with change of tool setting angle ϕ ($\tau=3$, $\varepsilon=0.6$).

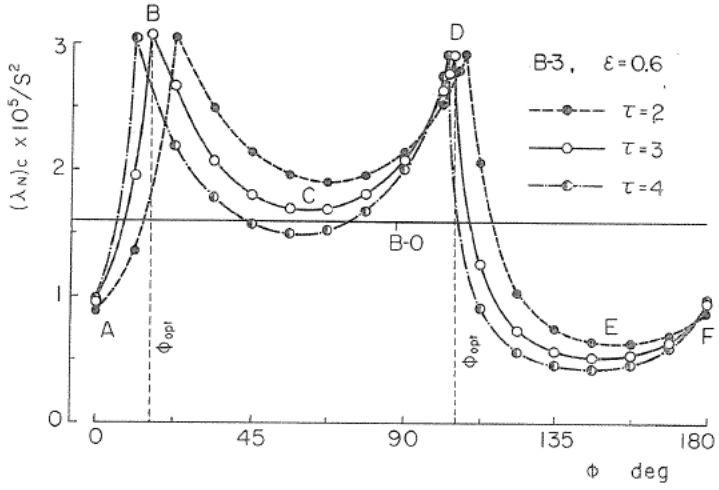

FIG. 5. Variation of stability boundary $(\lambda_N)_c$ with change of tool setting angle (*B*-3, $\varepsilon=0.6$, τ is varied).

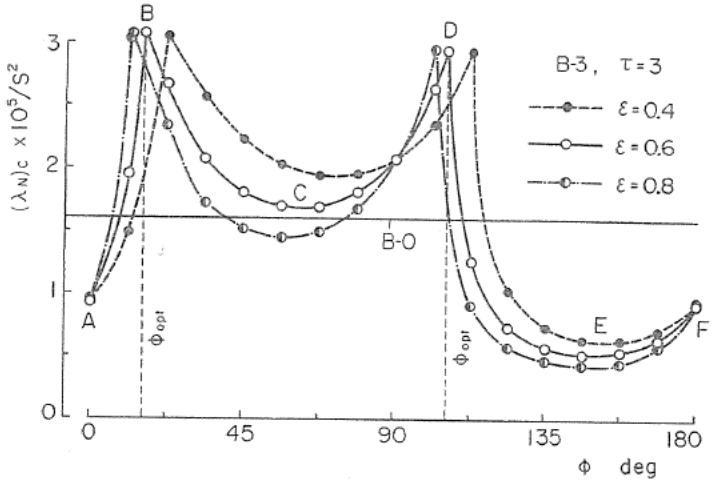

FIG. 6. Variation of stability boundary $(\lambda_N)_c$ with change of tool setting angle ϕ (B-3, $\tau=3$, ε is varied).

Meanwhile, for B-1, B-2 and B-3 boring bar systems in Fig. 4, $(\lambda_N)_c$ makes an interesting change with a tool setting angle ϕ, due to the directional characteristics of vibrational properties. That is to say, the value of $(\lambda_N)_c$ becomes maximum at the tool setting angle B (the first order of ϕ_{opt}) and D (the second order of ϕ_{opt}). It is obvious that within this calculation the maximum value of $(\lambda_N)_c$ becomes large with the increase of the frequency ratio $r=p_y/p_x$ and for every boring bar the maximum value of $(\lambda_N)_c$ at B is slightly greater than that at D. These maximum values are considerably larger than those of system B-0, the minimum value at C is larger than at E and the difference between these minimum values becomes large with increase of frequency ratio r. This fact may be closely related with the magnitudes of natural frequencies and damping coefficients in both x and y directions.

Next, it is clear in Figs. 5 and 6 that the relations between the stability boundary $(\lambda_N)_c$ and the tool setting angle ϕ have a strong resemblance to those in Fig. 4. However, it is seen that the value of ϕ_{opt} are considerably connected with the cutting conditions, *i.e.*, τ and ε, but that the maximum values of $(\lambda_N)_c$ at ϕ_{opt} are almost constant, independently of the change in τ or ε. Meanwhile, the minimum values of $(\lambda_N)_c$ decrease with the increase of τ or ε.

From the above discussion, it is clear that there are optimum tool setting angles for the effective prevention of chatter vibration in boring bars having directional characteristics in vibrational properties, and it is expected that the chatter behaviour will be remarkably improved if the good use of the directional characteristics of the boring bar is made.

However, the above discussion is based on the calculations for the boring bars which have the almost equal value of $\sqrt{(p_x^2+p_y^2)/2}$. As a result, the larger the ratio $r=p_y/p_x$ is, the larger cross sectional area the boring bars have, as seen in Fig. 1. The fact seen in Fig. 4 that $(\lambda_N)_{max}$ increases with the increase of r may be caused by the above mentioned effect to some degree. To examine this effect, the stability boundary $(\lambda_N)_c$ is again calculated for circular sectioned boring

bars which have diameters equal to the maximum size of B–1, B–2 and, B–3, and are shown in Fig. 4 by the lines B-10, B-20 and B-30. It is clear in the figure that $(\lambda_N)_c$ in the boring bars, having directional characteristics, is considerably larger than that in the circular sectioned boring bars at ranges of tool setting angle neighboring ϕ_{opt}.

Next, the frequency f can be calculated from Eq. (21). As an example, the result for the B–3 system is shown in Fig. 4 by fine solid lines. Two straight lines indicate the natural frequencies $f_x=p_x/2\pi$, $f_y=p_y/2\pi$ of the B–3 system. It is recognized in the figure that the tool setting angle is divided into two ranges, one is the range in which the chatter occurs with frequency closely equal to f_x, the other is the range in with the chatter occurs with frequency closely equal to f_y, furthermore, the tool setting angle where the chatter frequency f changes abruptly agrees with ϕ_{opt} approximately.

To discuss the interesting results about the stability boundary $(\lambda_N)_c$ and chatter frequency f in detail, the relation between α, f and ϕ is calculated by the system B–3, using Eqs. (14), (16) and (17), and is shown in Figs. 7 and 8. Fig. 7 is for the case when the system becomes unstable at some ranges of ϕ, and is for $\lambda_N=1.09\times10^5$ 1/sec^2. Fig. 8 is for $\lambda_N=3.28\times10^5$ 1/sec^2, and corresponds to the case when the system becomes unstable in all ranges of ϕ.

It is seen in Fig. 7 that α_1, α_2 are both negative within the range A–B, and then that the system is stable and the vibrations with frequencies close to f_x, f_y damp out. In the range B–C, however, α_1 is positive, hence the vibrations set up with frequency f_1 nearly equal to f_x.

Next, it is seen in Fig. 8 that either α_1 or α_2 is positive in all tool setting angles ϕ, and the system is unstable for the whole range. In the range A–B and D–E–F, the vibration occurs with frequency f_1, and within the range B–C–D with f_2. However, these frequencies f_1 and f_2 are considerably different from the natural frequencies f_x, f_y.

It may be noted in Eig. 8 that the magnitudes of α_1 and α_2 are reversed at B and D. This fact is closely connected with $(\lambda_N)_c$ becoming maximum at B and

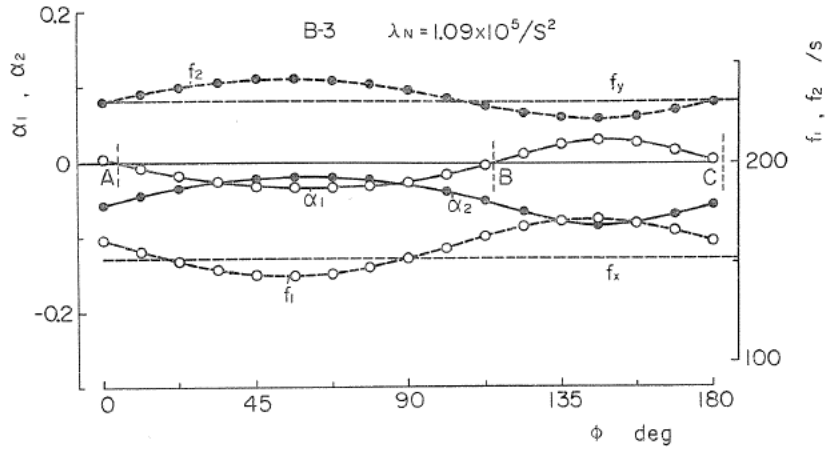

FIG. 7. Variation of increments or decrements α_1, α_2 and frequencies f_1, f_2 with change of tool setting angle ϕ (B–3, $\tau=3$, $\varepsilon=0.6$).

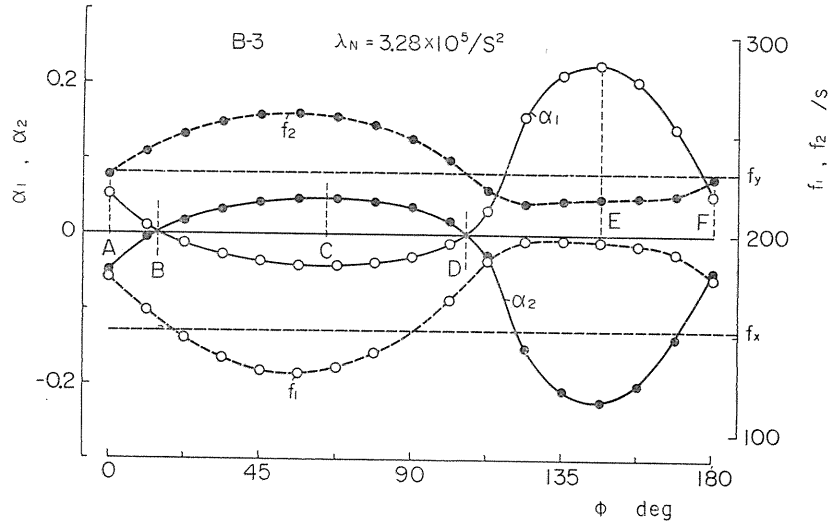

FIG. 8. Variation of increments or decrements α_1, α_2 and frequencies f_1, f_2 with change of tool settig angle ϕ (B-3, $\tau=3$, $\varepsilon=0.6$).

D in Fig. 4. It is further interesting to compare Fig. 8 with the B-3 curve in Fig. 4. The fact that α_2 or α_1 becomes maximum at C or E in Fig. 8 corresponds to the result that $(\lambda_N)_c$ becomes minimum at C and E of Fig. 4. Taking this into considerarion, it is understood that the minimum value of $(\lambda_N)_c$ at E is smaller than that in C in Fig. 4.

2.1.3. Optimum tool setting angle

On the basis of Eq. (20), the tool setting angle at which $(\lambda_N)_c$ becomes maximum, that is, the optimum tool setting angle ϕ_{opt} for the prevention of chatter can be calculated.

Expanding Eq. (20) into a polynomial of λ_0, and using Eq. (12), a cubic equation for λ_0 is obtained as follows:

$$A(\phi)\lambda_0^3 + B(\phi)\lambda_0^2 + C(\phi)\lambda_0 + D = 0 \tag{24}$$

where $A(\phi)$, $B(\phi)$ and $C(\phi)$ are the functions of tool setting angle ϕ and D is a constant free from ϕ.

Differentiating Eq. (24) by ϕ, then

$$d\lambda_0/d\phi = -\{dA(\phi)/d\phi\cdot\lambda_0^3 + dB(\phi)/d\phi\cdot\lambda_0^2 + dC(\phi)/d\phi\cdot\lambda_0\}/\{3A(\phi)\lambda_0^2 + 2B(\phi)\lambda_0 + C(\phi)\} \tag{25}$$

Referring to Figs. 4, 5 and 6, it is obvious that Eq. (24) is not differentiable at the point where λ_0 (that is, $(\lambda_N)_c$) becomes maximum. However, at the left side of the maximum value $d\lambda_0/d\phi>0$, and at the right side $d\lambda_0/d\phi<0$. Hence, the optimum tool setting angle ϕ_{opt} can be calculated by seeking the point where the sign of $d\lambda_0/d\phi$ changes from positive to negative by the method of numerical calculation.

As an example, Figs. 9 and 10 show the results of the calculation of the first

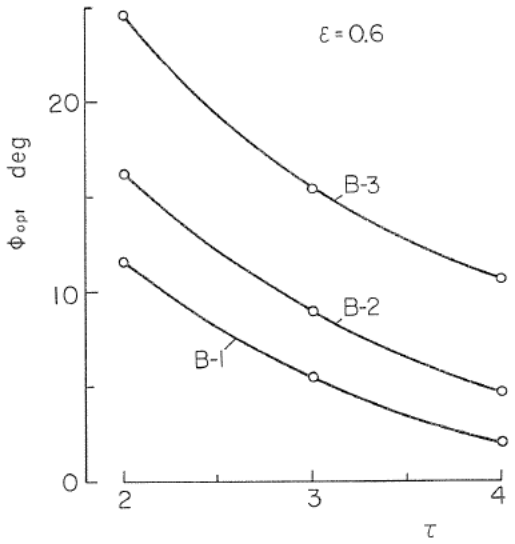

FIG. 9. Relation between optimum tool setting angle ϕ_{opt} and ratio τ for various boring bars ($\varepsilon=0.6$).

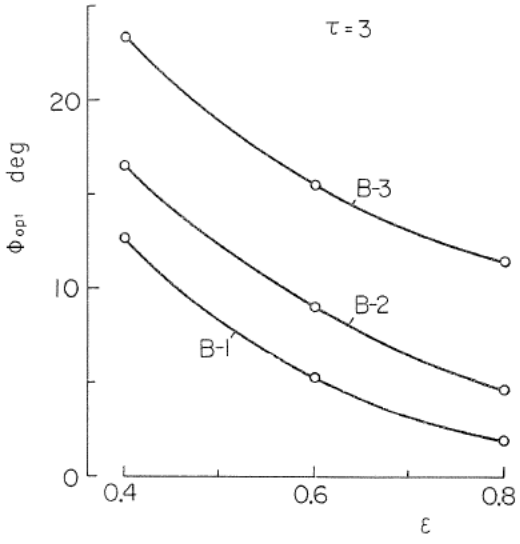

FIG. 10. Relation between optimum tool setting angle ϕ_{opt} and ratio ε for various boring bars ($\tau=3$).

order of ϕ_{opt}. It is clear in Fig. 9, where τ is changed, that ϕ_{opt} decreases with the increase of τ for each boring bar system. It is also seen in Fig. 10, where ε is changed, that ϕ_{opt} decreases with the increase of ε. Therefore, τ and ε may have a similar influence on ϕ_{opt}. It may be noted that the greater the frequency ratio r is, the greater ϕ_{opt} is.

From the above discussion, it is clear that chatter behaviour is improved considerably by using a boring bar having directional characteristics in vibrational properties, and that there are optimum directional characteristics and odtimum tool setting angle for the prevention of chatter vibration.

2.2. Experimental result

To ascertain the above theoretical analysis, the following experiments are carried out.

Four boring bars having different amounts of directional characteristics are made (See Fig. 1 and Table 1), and a cutting tool (rake angle: 0°, side clearance angle: 6°, nose radius: 0.5 mm) is set to each bar. Boring operations are carried out such cutting conditions that the cutting velocity is about 30 m/min, the feed rate is 0.1 mm/rev, which is held constant, and the depth of cut is changed for various tool setting angles. The vibrations of x and y directions are measured electrically by the strain gauges AG 1~4 in Fig. 1. The strain gauges AG 1, 2 are for measuring the vibration of the boring bar in x direction, and AG 3, 4 are for measuring that in y direction, respectively.

Figs. 11 and 12 show examples of the chatter vibration in both x and y directions of the B-3 system for various tool setting angles.

Fig. 13 shows an example of the relations between the amplitude of chatter and the depth of cut obtained from many experimental photographs for B-3. In

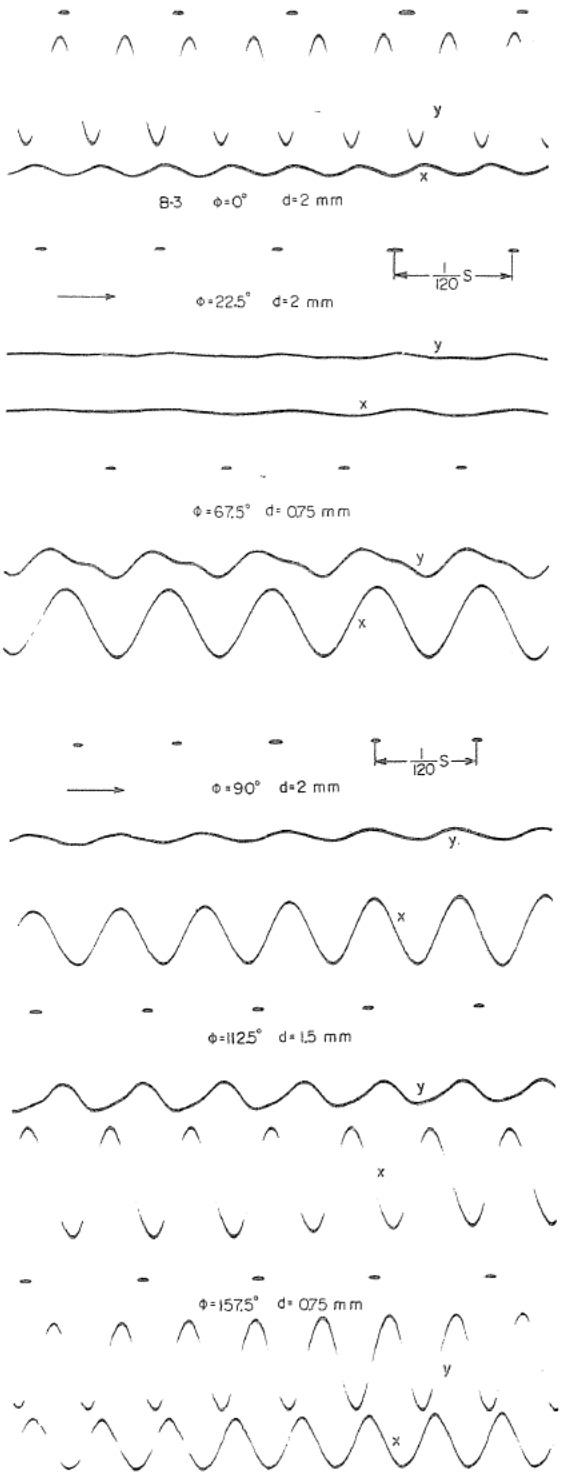

FIG. 11. Experimental records of chatter vibration.

FIG. 12. Experimental records of chatter vibration.

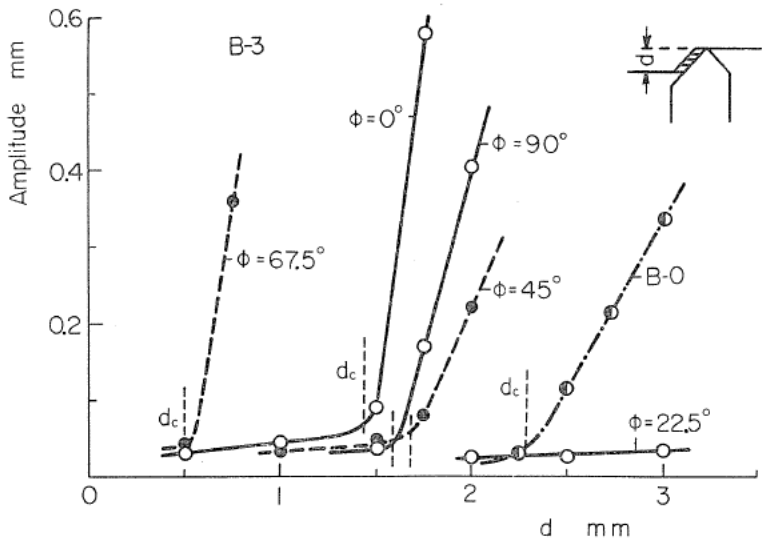

FIG. 13. Variation of amplitude with change of depth of cut d for various tool setting angles ϕ (B-3, B-0).

the figure, the experimental result for B-0 is shown by the chain line, too, for reference. From the amplitude-depth of cut curves in the figure, the critical depth of cut d_c at which the chatter vibration is set up, can be obtained experimentally for various tool setting angles. Here, it must be noted that the critical depth of cut d_c is equivalent to $(\lambda_N)_c$ in the theoretical analysis.

Fig. 14 shows the relations between d_c and ϕ for each boring bar. Comparing this experimental result with the corresponding theoretical resut in Fig. 4, it is obvious that both results show a closely similar tendency. Namely, for B-0 the critical depth of cut d_c is constant regardless of the tool setting angle ϕ. For B-2 and B-3, there are two tool setting angles at which d_c becomes maximum and these optimum tool setting angles ϕ_{opt} are in close agreement with those of calculations. Moreover, the value of $(\lambda_N)_c$ at the first order of ϕ_{opt} is considerably larger than that at the second order of ϕ_{opt}, and this fact corresponds with the calculational result in Fig. 4. For the B-1 system, however, the existence of the second order of ϕ_{opt} cannot be recognized, which may be considered to be due to the following fact. The experiments shown in Fig. 14 are carried out in oblique cutting conditions. The feed component of the cutting force may have an influence to some extent on $(\lambda_N)_c$ especially for such a system as B-1 in which the frequency ratio r is small. In the theoretical analysis, however, the feed component of the cutting force is neglected.

From the above considerations, it is ascertained that the analytical results are in good agreement with the experimental results quantitatively.

Fig. 15 shows an example of the vibrational loci of boring bar obtained for B-3 from the experimental photographs as shown in Figs. 11 and 12. It is seen in each locus that the frequencies in the x and y directions are equal in spite of the directional characteistics of boring bar. The shape of the vibrational locus is remarkably influenced by the tool setting angle ϕ. In the case of $\phi=0°$, the

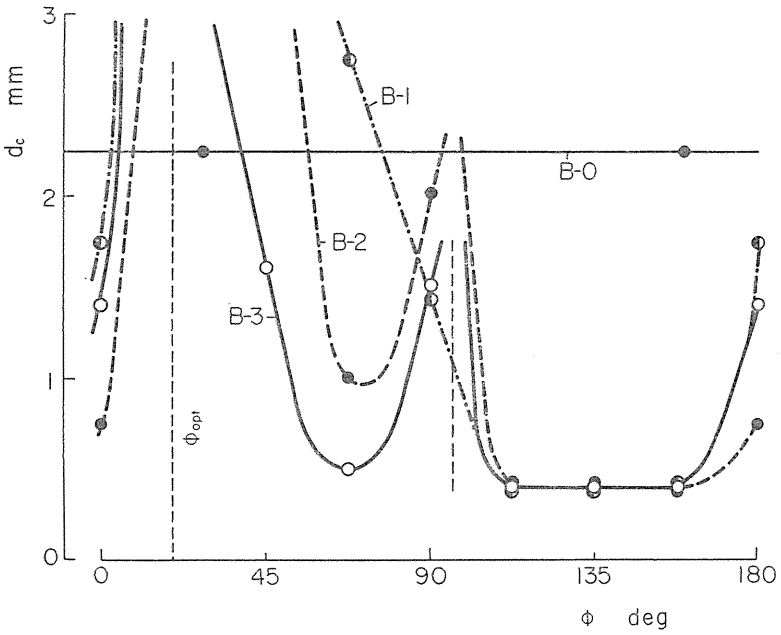

FIG. 14. Experimental results of critical depth of cut d_c for various tool setting angle ϕ.

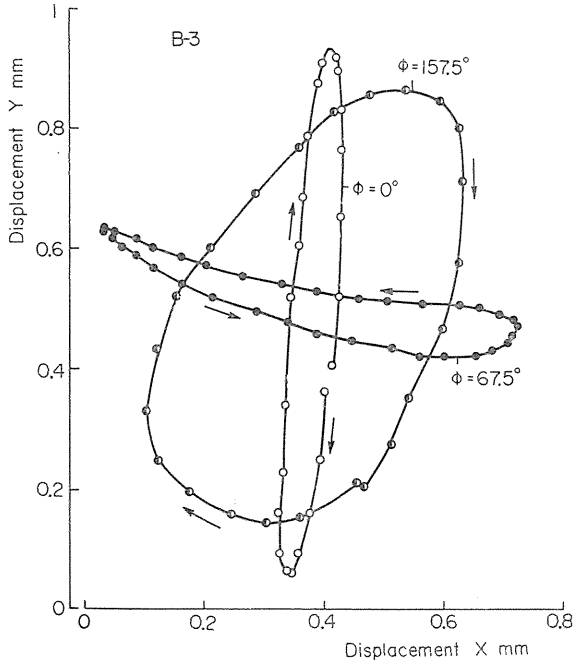

FIG. 15. Vibrational loci of boring bar for various tool setting angles ϕ (B-3).

amplitude in y direction is quite large compared with that in x direction, and the rotational direction of a vibrational locus is the same as for the boring bar. Next, in the case of $\phi=67.5°$ (which is larger than the first order of ϕ_{opt}), the amplitude in x direction is quite large, and the rotational direction is the reverse of that of the boring bar. Last, in the case of $\phi=157.5°$ (which is larger than the second order of ϕ_{opt}), the amplitude in y direction increases again, and the rotational direction of the locus agrees with that of the boring bar. It is very interesting that the phenomenon discussed above corresponds to the facts considered in Fig. 8.

2.3. Conclusion

The stability boundary for chatter vibration in boring operation is introduced as the function of vibrational properties of boring bar and the cutting conditions. On the basis of the stability boundary, some considerations for the prevention of chatter are made.

As a result, it is ascertained that chatter behaviour is improved considerably by using a boring bar having directional characteristics in vibrational properties, and that there are optimum directional characteristics and optimum tool setting angles for the prevention of chatter vibration.

3. Some Considerations on Prevention of Chatter Vibration in Multi-edge Rotary Cutting Tool, 1[11)13)]

It may be inevitable that the multi-edge rotary cutting tools such as drill, tap and reamer have directional characteristics in the vibrational properties (that is, stiffness, natural frequency, damping coefficient), owing to the structure of the tools. Fig. 16 is an example showing the bending stiffness k of a twist drill for various loading directions θ. It is seen in the figure that the k–θ curves for two drills used in the experiment are fairly different and the maximum and minimum values of k are not equal, and further that the setting angles of two cutting edges C_1, C_2 against the tool axis are not equal for two drills.

In this chapter, the stability boundary of chatter is introduced theoretically as the function of the tool setting angles against the directional characteristics and the various cutting conditions, and is ascertained experimentally. On the basis of these results, the concrete means for the prevention of the chatter vibration in multi-edge rotary cutting tool is suggested.

3.1. Analysis

3.1.1. Equation of motion and stability boundary

First, the differential equation representing the chatter vibration in multi-edge rotary cutting tools with directional characteristics as shown in Fig. 17 will be determined for the general case that n cutting edges are placed in arbitrary setting angles, and the stability boundary of chatter will be discussed theoretically, using the same method as in the analysis of the chatter vibration in the boring bar of the previous chapter.

For the sake of simplicity, multi-edge rotary cutting tool is regarded as a lumped mass system with two degrees of freedom, and analysis is made for orthogonal cutting. The analytical results, however, include other cutting operations.

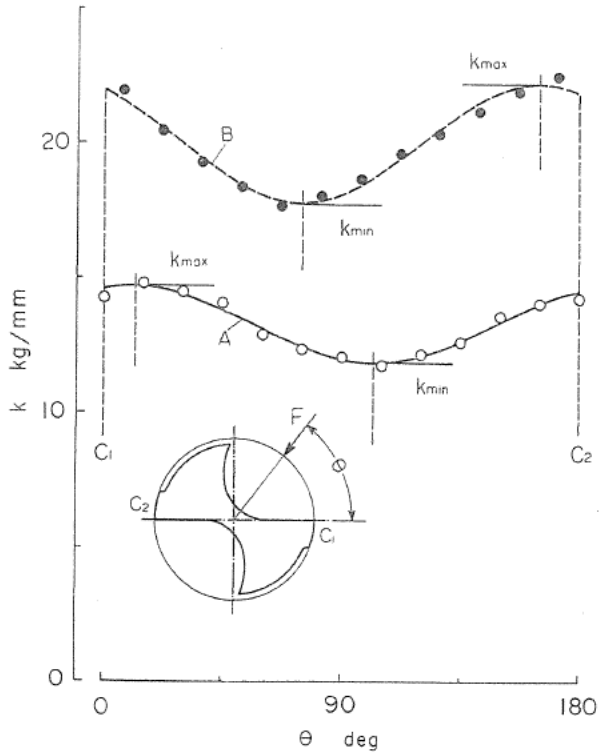

FIG. 16. Load test of twist drill.

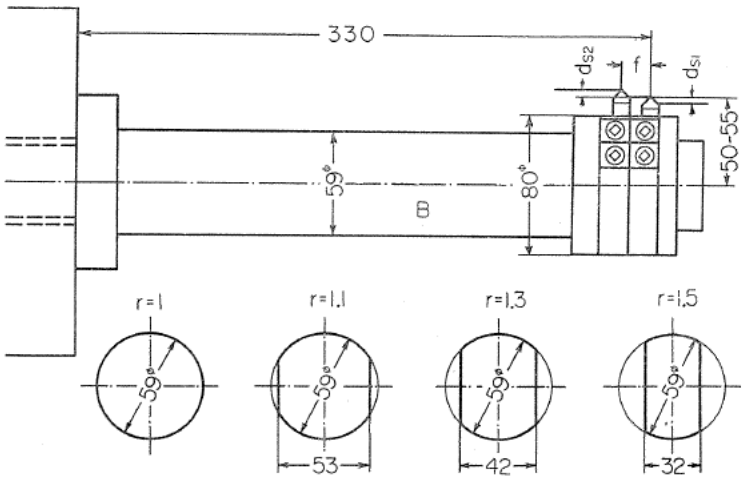

FIG. 17. Diagram of cutting tools.

Fig. 18 shows the coordinate axis of the tools having two cutting edges. In the figure, center A of the tool displaces to point O under the action of the cutting force in a cutting operation. Taking this point O as the origin, x-axis is determined in the direction of the least stiffness of the tool, and y-axis in the

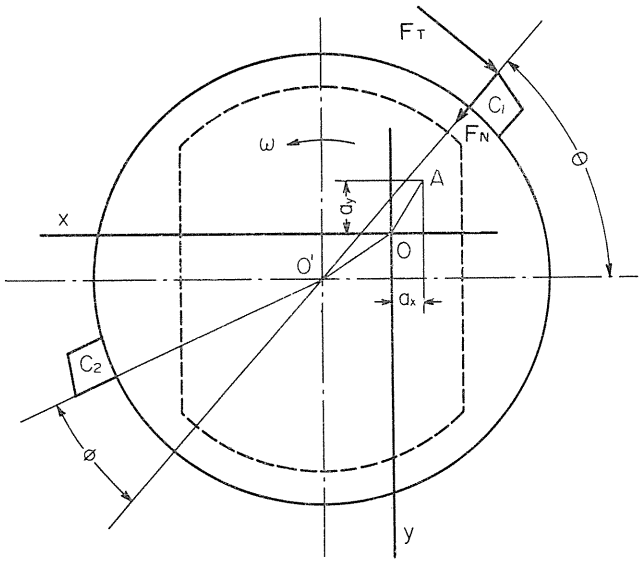

FIG. 18. Rotational coordinate system fixed to cutting tools.

direction of the greatest. This coordinate system rotates with the same angular velocity as a tool. When the cutting operation is steady, the tool displaces to the amount of a_x along the x-axis and a_y along the y-axis by the resultant cutting force respectively. If the corresponding depth of cut for each cutting edge is denoted by d_{si}, then

$$\left.\begin{aligned}\sum_{i=1}^{n} F_{sxi}(d_{si}) &= (k_x - m\omega^2)a_x \\ \sum_{i=1}^{n} F_{syi}(d_{si}) &= (k_y - m\omega^2)a_y\end{aligned}\right\} \tag{26}$$

where $F_{sxi}(d_{si})$, $F_{syi}(d_{si})$ represent the components of cutting force in x and y directions, $k_x a_x$, $k_y a_y$ are the spring forces in both directions, and $-m\omega^2 a_x$, $-m\omega^2 a_y$ are the centrifugal forces respectively.

Next, the cutting force acting in one cutting edge C_i during vibration will be introduced. Representing the angle between the x-axis and the cutting edge setting direction by θ_i, the depth of cut for cutting edge C_i during vibration can be expressed as follows:

$$d_i = d_{si} - (x\cos\theta_i + y\sin\theta_i) \tag{27}$$

Assuming that each component of cutting force is proportional to the depth of cut, and that the cutting force acts on the vibratory system with constant time lag on the basis of the privous experimental results[4] regarding the cause of chatter vibration, the thrust force F_{Ni} and the cutting force F_{Ti} can be written as follows:

$$\left.\begin{aligned}F_{Ni} &= K_{Ni}\{d_{si} - x(t-H)\cos\theta_i - y(t-H)\sin\theta_i\} \\ F_{Ti} &= K_{Ti}\{d_{si} - x(t-h)\cos\theta_i - y(t-h)\sin\theta_i\}\end{aligned}\right\} \tag{28}$$

where H and h indicate the time lags of the thrust and cutting force respectively, and K_{Ni} and K_{Ti} are the proportional coefficients of the cutting and the thrust force respectively. Hence, K_{Ni}, K_{Ti} are closely related to the cutting conditions (that is, material being cut, geometry of cutting edge, width of cut and so on).

The x and y components of the cutting force acting on the cutting edge C_i, that is, F_{xi} and F_{yi}, can be written as functions of F_{Ni} and F_{Ti} as follows:

$$\left.\begin{aligned} F_{xi} &= F_{Ni}\cos\theta_i - F_{Ti}\sin\theta_i \\ F_{yi} &= F_{Ni}\sin\theta_i + F_{Ti}\cos\theta_i \end{aligned}\right\} \tag{29}$$

It is justifiable that the time lags H, h of the cutting force are such small amounts[4] that $x(t-H)$, $y(t-H)$, etc. are approximated as follows:

$$\left.\begin{aligned} x(t-H) &= x - H\dot{x},\ y(t-H) = y - H\dot{y} \\ x(t-h) &= x - h\dot{x},\ y(t-h) = y - h\dot{y} \end{aligned}\right\} \tag{30}$$

Using Eqs. (28), (29), (30), F_{xi}, F_{yi} are obtained as follows:

$$\left.\begin{aligned} F_{xi} &= F_{sxi}(d_{si}) - K_{Ni}x\cos^2\theta_i - (K_{Ni}y - K_{Ti}x)\sin\theta_i\cos\theta_i + K_{Ti}y\sin^2\theta_i \\ &\quad + K_{Ni}H\dot{x}\cos^2\theta_i + (K_{Ni}H\dot{y} - K_{Ti}h\dot{x})\sin\theta_i\cos\theta_i - K_{Ti}h\dot{y}\sin^2\theta_i \\ F_{yi} &= F_{syi}(d_{si}) - K_{Ti}x\cos^2\theta_i - (K_{Ni}x + K_{Ti}y)\sin\theta_i\cos\theta_i - K_{Ni}y\sin^2\theta_i \\ &\quad + K_{Ti}h\dot{x}\cos^2\theta_i + (K_{Ni}H\dot{x} + K_{Ti}h\dot{y})\sin\theta_i\cos\theta_i + K_{Ni}H\dot{y}\sin^2\theta_i \end{aligned}\right\} \tag{31}$$

where

$$\left.\begin{aligned} F_{sxi}(d_{si}) &= K_{Ni}d_{si}\cos\theta_i - K_{Ti}d_{si}\sin\theta_i \\ F_{syi}(d_{si}) &= K_{Ni}d_{si}\sin\theta_i + K_{Ti}d_{si}\cos\theta_i \end{aligned}\right\} \tag{32}$$

Using the above equations, the differential equation representing the chatter vibration occuring in multi-edge rotary cutting tool can be derived by the rotational coordinate system as follows:

$$\left.\begin{aligned} m\ddot{x} + c_x\dot{x} + (k_x - m\omega^2)(x + a_x) - 2m\omega\dot{y} &= \sum_{i=1}^{n} F_{xi} \\ 2m\omega\dot{x} + m\ddot{y} + c_y\dot{y} + (k_y - m\omega^2)(y + a_y) &= \sum_{i=1}^{n} F_{yi} \end{aligned}\right\} \tag{33}$$

where m is the equivalent mass of the tool system and it is assumed that the values of m in x and y directions are equal; c_x, c_y are the damping cofficients and k_x, k_y are the spring constants in both directions respectively; ω is the angular velocity of the tool.

Setting

$$\left.\begin{aligned} &c_x/m = 2n_x,\ c_y/m = 2n_y,\ n_y/n_x = q,\ k_x/m = p_x^2,\ k_y/m = p_y^2, \\ &p_y/p_x = r,\ h/H = \varepsilon,\ K_{Ni}/m = \lambda_{Ni},\ K_{Ti}/m = \lambda_{Ti}, \\ &\sum_{i=1}^{n}\lambda_{Ni}/n = \lambda_N,\ \sum_{i=1}^{n}\lambda_{Ti}/n = \lambda_T,\ \lambda_T/\lambda_N = \tau,\ \lambda_{Ni}/\lambda_N = g_i \end{aligned}\right\} \tag{34}$$

where g_i is the cutting factor of each cutting edge indicating the contributing rate to the cutting operation, and is written as follows:

$$\sum_{i=1}^{n} g_i = n \tag{35}$$

Using Fqs. (26), (31), (32), (34), Eq. (33) becomes,

$$\left.\begin{aligned} &\ddot{x} + a_1\dot{x} + a_2 x + a_3\dot{y} + a_4 y = 0 \\ &b_1\dot{x} + b_2 x + \ddot{y} + b_3\dot{y} + b_4 y = 0 \end{aligned}\right\} \tag{36}$$

where

$$\left.\begin{aligned} a_1 &= 2n_x - \lambda_N\Big(H\sum_{i=1}^{n} g_i\cos^2\theta_i - h\sum_{i=1}^{n} g_i\sin\theta_i\cos\theta_i\Big) \\ a_2 &= p_x^2 - \omega^2 + \lambda_N\Big(\sum_{i=1}^{n} g_i\cos^2\theta_i - \tau\sum_{i=1}^{n} g_i\sin\theta_i\cos\theta_i\Big) \\ a_3 &= -2\omega - \lambda_N\Big(H\sum_{i=1}^{n} g_i\sin\theta_i\cos\theta_i - \tau h\sum_{i=1}^{n} g_i\sin^2\theta_i\Big) \\ a_4 &= \lambda_N\Big(\sum_{i=1}^{n} g_i\sin\theta_i\cos\theta_i - \tau\sum_{i=1}^{n} g_i\sin^2\theta_i\Big) \\ b_1 &= 2\omega - \lambda_N\Big(H\sum_{i=1}^{n} g_i\sin\theta_i\cos\theta_i + \tau h\sum_{i=1}^{n} g_i\cos^2\theta_i\Big) \\ b_2 &= \lambda_n\Big(\sum_{i=1}^{n} g_i\sin\theta_i\cos\theta_i + \tau\sum_{i=1}^{n} g_i\cos^2\theta_i\Big) \\ b_3 &= 2n_y - \lambda_N\Big(H\sum_{i=1}^{n} g_i\sin^2\theta_i + \tau h\sum_{i=1}^{n} g_i\sin\theta_i\cos\theta_i\Big) \\ b_4 &= p_y^2 - \omega^2 + \lambda_N\Big(\sum_{i=1}^{n} g_i\sin^2\theta_i + \tau\sum_{i=1}^{n} g_i\sin\theta_i\cos\theta_i\Big) \end{aligned}\right\} \tag{37}$$

Now, the solution of Eq. (36) is assumed as follows:

$$\left.\begin{aligned} &x = x_0 e^{st},\ y = y_0 e^{st} \\ &s = \alpha + j\beta,\ j = \sqrt{-1} \end{aligned}\right\} \tag{38}$$

The characteristic equation of the vibratory system can be obtained as follows:

$$\left.\begin{aligned} &s^4 + A_1 s^3 + A_2 s^2 + A_3 s + A_4 = 0 \\ &A_1 = a_1 + b_3 \\ &A_2 = a_1 b_3 + a_2 + b_4 - a_3 b_1 \\ &A_3 = a_1 b_4 + a_2 b_3 - a_3 b_2 - a_4 b_1 \\ &A_4 = a_2 b_4 - a_4 b_2 \end{aligned}\right\} \tag{39}$$

Reffering to the Hurwitz criterion, the following expression for the stability boundary of chatter vibration can be obtained.

$$A_3(A_1 A_2 - A_3) - A_1^2 A_4 = 0 \tag{40}$$

In Eqs. (40), (39), (37), parameters p_x, p_y, n_x, n_y, ω, θ_i, g_i, H, h, τ are determined by the vibrational properties or the cutting conditions. Hence, regarding these parameters as assigned, the critical value of λ_N which gives the excitation boundary of chatter can be determined from Eq. (40) as follows:

$$(\lambda_N)_c = \lambda_N(p_x, p_y, n_x, n_y, \omega, \theta_i, g_i, H, h, \tau) \tag{41}$$

Therefore, the chatter vibration should be brought out in such cutting conditions that the magnitude of λ_N is greater than the critical value $(\lambda_N)_c$.

3.1.2. Numerical calculation and consideration (Case of $n=2$, $g_1=g_2=1$)

First, the stability boundary $(\lambda_N)_c$ in the case of tools with two cutting edges ($n=2$) will be examined, using Eq. (41). The vibrational properties of each vibratory system shown in Fig. 17 are acqired from the free vibration test. The results are listed collectively in Table 2. Fig. 19 shows the relation between the damping coefficients n and the natural angular frequency p of these systems. It is seen in this figure that there is a good liner relationship between n and p^2. Hence, numerical calculation in this paper is carried out based upon this relation ($n \propto p^2$).

The cutting factor g_i depends generally on the cutting edge setting conditions (both axial and radial) and the dimensions of each cutting edge. For example, when the axial distance of two cutting edges f (See Fig. 17) is greater than the

TABLE 2. Vibrational Properties of Cutting Tools

$r=p_y/p_x$	p_x (rad/s)	p_y (rad/s)	n_x (1/s)	n_y (1/s)
$r=1$	1855	1855	74.3	74.3
$r=1.1$	1618	1771	54.5	67.7
$r=1.3$	1235	1606	32.9	55.6
$r=1.5$	963	1445	20.0	45.1

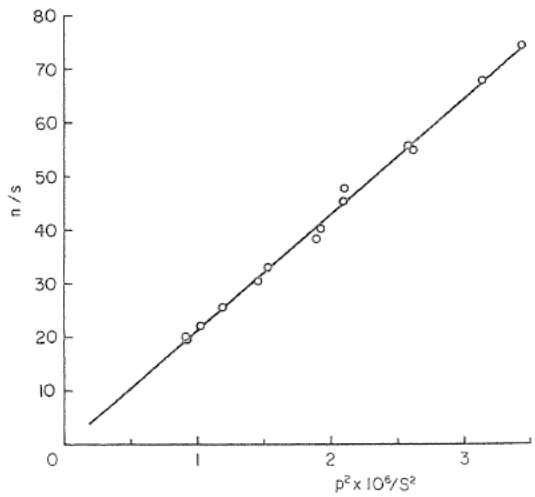

FIG. 19. Relation between damping coefficient n and natural angular frequency p.

feed of tool or workpiece, and the depth of cut of each edge is equal, $g_1=g_2=1$ for arbitrary condition of each cutting edge.

Accordingly, as a standard case of consideration, the stability boundary of the tools with two cutting edges is investigated for the case that $g_1=g_2=1$, that is, the cutting factors of two cutting edges are equal.

For example, Figs. 20~24 show the relations between the stability boundary $(\lambda_N)_c$ and the various cutting edge setting conditions, which are obtained from Eq. (41). Here, representing the cutting edge setting angle of C_1 (that is, θ_1) by θ, that of C_2 (that is, θ_2) is expressed by $\theta_2=180+(\theta-\phi)$, where, ϕ indicates the

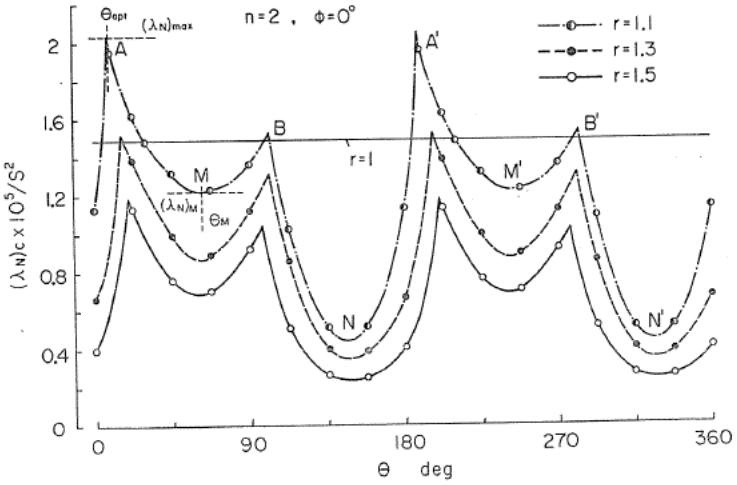

FIG. 20. Variation of stability boundary $(\lambda_N)_c$ with change of cutting edge setting angle θ ($\phi=0°$).

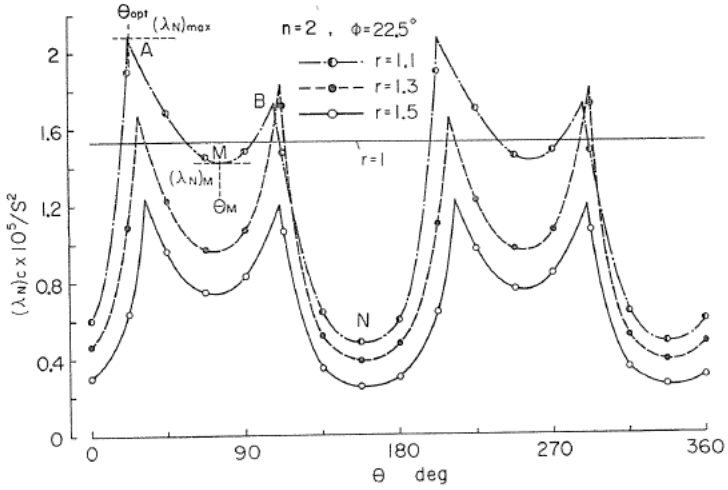

FIG. 21. Variation of stability boundary $(\lambda_N)_c$ with change of cutting edge setting angle θ ($\phi=22.5°$).

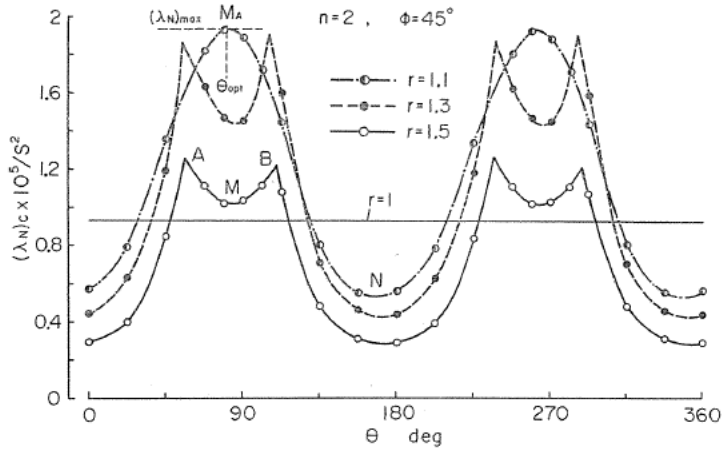

FIG. 22. Variation of stability boundary $(\lambda_N)_c$ with change of cutting edge setting angle θ ($\phi=45°$).

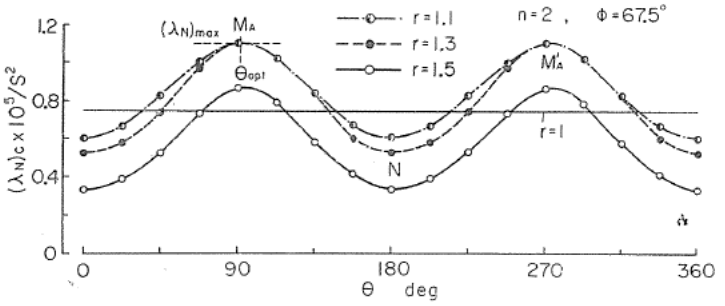

FIG. 23. Variation of stability boundary $(\lambda_N)_c$ with change of cutting edge setting angle θ ($\phi=67.5°$).

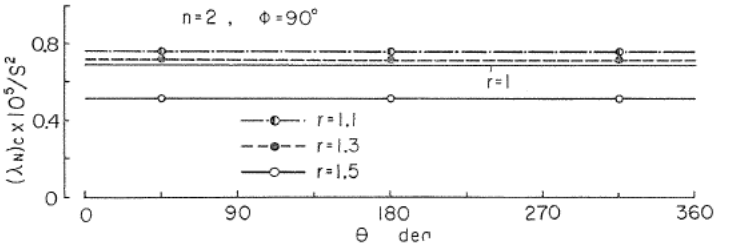

FIG. 24. Variation of stability boundary $(\lambda_N)_c$ with change of cutting edge setting angle θ ($\phi=90°$).

shifted angle from the symmetrical setting position of both cutting edges (See Fig. 18). In these calculations, the following numerical values are used referring to many previous experimental data, *i.e.*, $H=0.0005$ sec, $\varepsilon=h/H=0.6$, $\tau=3$. In Figs. 20~24, any vibratory system becomes unstable in such cutting conditions that the individual value of λ_N is larger than that of $(\lambda_N)_c$ predicted from the corresponding $(\lambda_N)_c \sim \theta$ curve.

In the tool which has no directional characteristics in vibrational properties (that is, $r=p_y/p_x=1$), the stability boundary $(\lambda_N)_c$ is independent of the cutting edge setting conditions, seen as fine solid lines in these figures.

Fig. 20 shows the relation between $(\lambda_N)_c$ and the various cutting edge setting angles θ against x-axis, when two cutting edges are arranged symmetrically. For $r=1.1$, $r=1.3$ and $r=1.5$ tool systems in Fig. 17, $(\lambda_N)_c$ makes an interesting change with the cutting edge setting angle θ, due to the directional characteristics of vibrational properties. That is to say, the value of $(\lambda_N)_c$ becomes maximum at the cutting edge setting angles A, A' (the first order of θ_{opt}) and B, B' (the second order of θ_{opt}). These optimum setting positions are a little ahead of the least stiffness directions ($\theta=0°$, $180°$) or the greatests tiffness ones ($\theta=90°$, $270°$) in the same rotational directions as that of the tool. It is obvious that within this calculation the maximum value $(\lambda_N)_{max}$ of the $r=1.1$ tool system is the greatest of all, and this greatest value is extremely greater than the stability boundary $(\lambda_N)_c$ at A, A' is fairly greater than that at B, B'.

Next, Figs. 21~24 show the relations between the stability boudary $(\lambda_N)_c$ and the cutting edge setting angle θ, where two cutting edges are shifted by the amount of $\phi=22.5°$, $45°$, $67.5°$ and $90°$ from the symmetrical setting position of both cutting edges respectively.

It is recognized in these figures that the $(\lambda_N)_c\sim\theta$ relations of these cases differ in features from that of $\phi=0°$. Namely, the cutting edge setting angle at which $(\lambda_N)_c$ becomes maximum moves rightwards in the figure, that is, the value of θ_{opt} becomes large with increase of the shifted angle ϕ. Furtheremore, for a large shifted angle ϕ, the value of $(\lambda_N)_c$ becomes maximum at only two cutting angles M_A, M_A', which lie between the first order of θ_{opt} and the second order of ϕ_{opt} (See the case of $\phi=45°$ and $r=1.1$). In the case of $\phi=90°$, the stability boundary $(\lambda_N)_c$ is independent of the cutting edge setting angle θ, regardless of the presence of the directional characteristics in the vibrational properties.

Figs. 25, 26 show the relation between the maximum value $(\lambda_N)_{max}$, the corresponding optimum cutting edge setting angle θ_{opt} and the shifted angle ϕ. In these figures, the ranges A-B, C-D and E-F correspond to the case where the

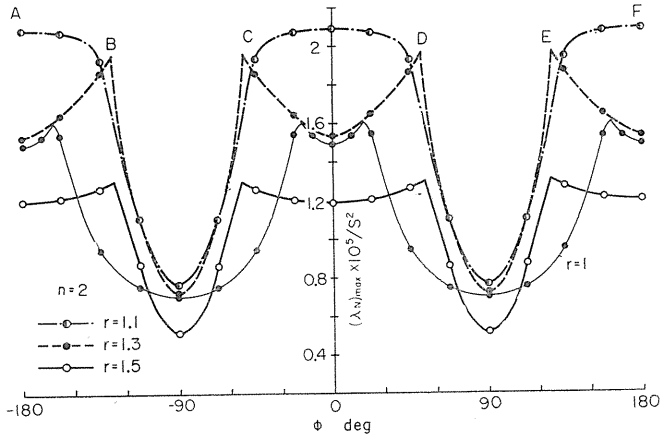

FIG. 25. Relation between maximum value $(\lambda_N)_{max}$ and shifted angle ϕ.

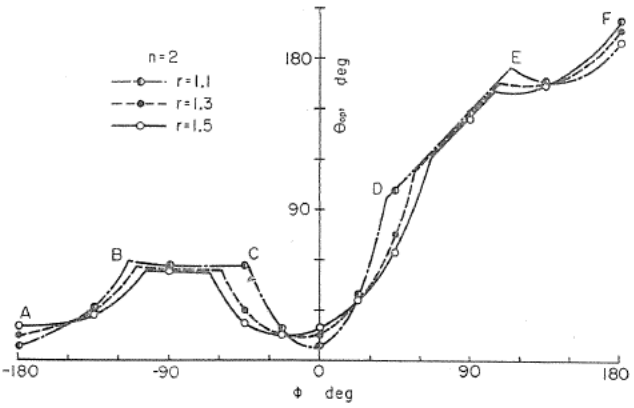

FIG. 26. Relation between optimum cutting edge setting angle θ_{opt} and shifted angle ϕ.

value $(\lambda_N)_c$ has four maximum values, and the ranges B–C, D–E correspond to the case where $(\lambda_N)_c$ has two maximum values.

It is obvious in Fig. 25 that the value of $(\lambda_N)_{max}$ become maximum and the chatter vibration can most effectively be prevented in $30°>\phi>-30°$ in case of the $r=1.1$ tool system, and at the critical shifted angle ϕ at which the number of the maximum values of $(\lambda_N)_c$ changes from four to two in case of the $r=1.3$, $r=1.5$ tool systems. However, in any tool systems $(\lambda_N)_{max}$ becomes minimum at $\phi=90°$ where both cutting edges lie in a rectangular position to each other, hence, this setting condition is an undesirable one to prevent the chatter vibration. From Figs. 25, 26, it is recognized that the chatter vibration of the multi-edge rotary cutting tool can remarkably be prevented in the tool system having suitable values of r, ϕ, θ.

Fig. 27 shows the relation between the maximum value $(\lambda_N)_{max}$ and the frequency ratio r. The value of $(\lambda_N)_{max}$ varies with the shifted angle ϕ, as shown in Fig. 25, nevertheless it is seen in Fig. 27 that $(\lambda_N)_{max}$ becomes maximum at almost the same frequency ratio, $r=r_{opt}$. This is a very favourable for the design of an effective tool to prevent the chatter vibration.

Next, the effect of the cutting conditions and the vibrational properties on $(\lambda_N)_{max}$, θ_{opt} and the optimum frequency ratio r_{opt} is examined in detail. As some examples, Figs. 28, 29 show the effect of the cutting force ratio τ and the damping coefficient n_x on the values of $(\lambda_N)_{max}$ and θ_{opt}.

It is obvious in Fig. 28 that the value of $(\lambda_N)_{max}$ is almost constant independently of τ, but, the corresponding value of θ_{opt} decreases with the increase of τ. Meanwhile, it is obvious in Fig. 29 that the value of $(\lambda_N)_{max}$ and the corresponding value of θ_{opt} increase with the increase of n_x.

Fig. 30 shows the relation between $(\lambda_N)_{max}$ and r for various values of n_x. The value of $(\lambda_N)_{max}$ becomes maximum at almost the same frequency ratio $r=r_{opt}$ for each value of n_x, as shown in the figure. And this magnitude of r_{opt} agrees nearly with that of Fig. 27.

It is clear from the above discussion that there exists the optimum frequency ratio, that is, the optimum tool configuration to prevent the catter vibration in

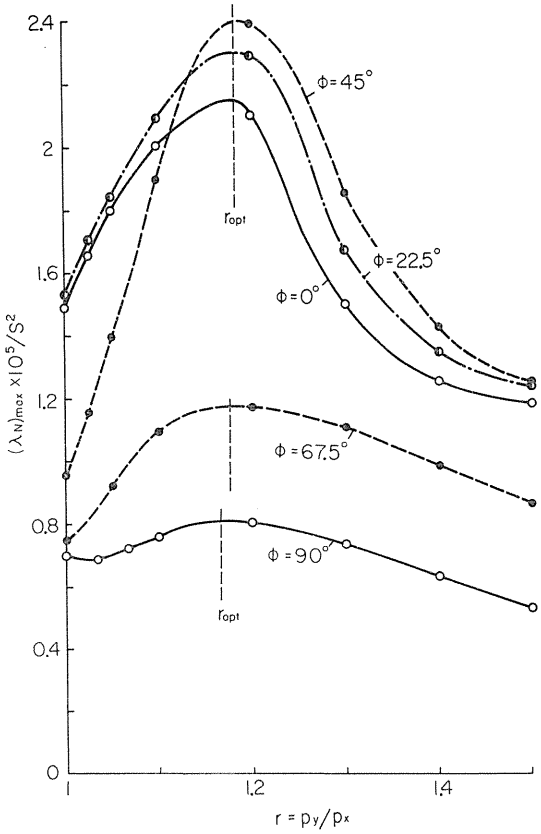

FIG. 27. Relation between maximum value $(\lambda_N)_{max}$ and frequency ratio r.

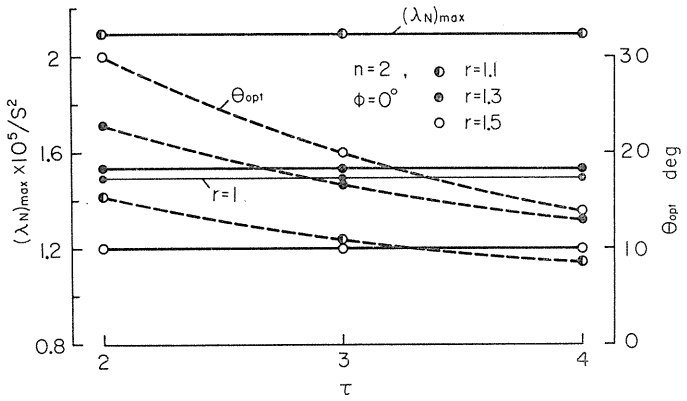

FIG. 28. Relation between maximum value $(\lambda_N)_{max}$, optimum cutting edge setting angle θ_{opt} and ratio τ.

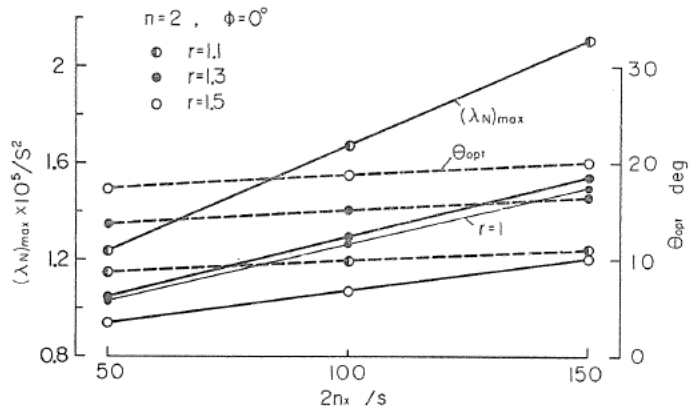

FIG. 29. Relation between maximum value $(\lambda_N)_{max}$, optimum cutting edge setting angle θ_{opt} and damping coefficient n_x.

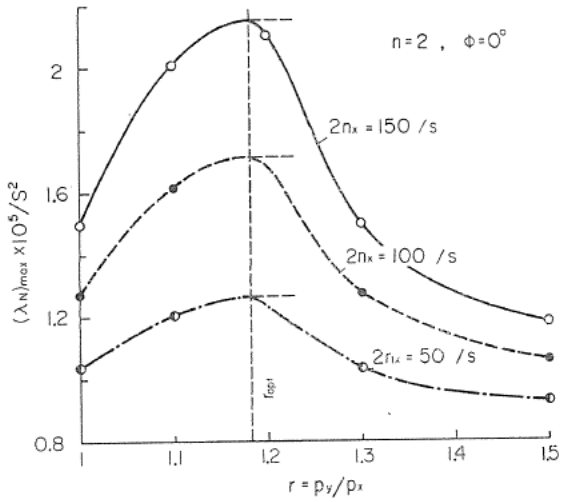

FIG. 30. Relation between maximum value $(\lambda_N)_{max}$ and frequency ratio r (damping coefficient n_x is varied).

the multi-edge rotary cutting tools, and this optimum tool configuration is not affected by the cutting conditions, the cutting edge setting conditions and the vibrational properties of the system. This is considered to be a favourable fact for the design of an effective tool to prevent the chatter vibration.

Thus, it is clear that there are optimum cutting edge setting angles for the effective prevention of the chatter vibration in multi-edge rotary cutting tools having the directional characteristics in vibrational properties, and it can be expected that the chatter behaviour will be remarkably improved if a good use of the directional characteristics of the tool is made. However, it may be noted that the tool displaces owing to the unbalance of cutting force acting on each cutting edge when both cutting edges are arranged unsymmetrically, *i.e.* $\phi \neq 0°$.

3.1.3. Effect of vibrational properties and cutting conditions on stability boundary $(\lambda_N)_c$

To discuss the above mentioned results about the stability boundary $(\lambda_N)_c$ in detail, the characteristic equation (39) is solved approximately using the undermentioned method.

Replacing s in Eq. (39) by $s^*-A_1/4$, next equation is obtained,

$$\left.\begin{aligned} &s^{*4}+\rho_1 s^{*2}+\rho_2 s^*+\rho_3=0 \\ &\rho_1=-\frac{3}{8}A_1^2+A_2 \\ &\rho_2=\frac{1}{8}A_1^3-\frac{1}{2}A_1A_2+A_3 \\ &\rho_3=-\frac{3}{256}A_1^4+\frac{1}{16}A_1^2A_2-\frac{1}{4}A_1A_3+A_4 \end{aligned}\right\} \tag{42}$$

The solution of Eq. (42) can be assumed as follows:

$$\left.\begin{aligned} &s_1^*=X+j(Y-Z),\ s_2^*=X-j(Y-Z) \\ &s_3^*=-X+j(Y+Z),\ s_4^*=-X-j(Y+Z) \end{aligned}\right\} \tag{43}$$

Substituting Eq. (43) in Eq. (42), using the relations between roots and coefficients of a fourth-degree polynomial equation and neglecting the higher order of s^*, the following equation on X is obtained.

$$32\,\rho_1X^4+4(\rho_1^2-4\,\rho_3)X^2-\rho_2^2=0 \tag{44}$$

X can be determined from Eq. (44) as follows:

$$\left.\begin{aligned} &X=\pm\sqrt{\frac{\sqrt{(\rho_1^2-4\,\rho_3)^2+8\,\rho_1\rho_2^2}-(\rho_1^2-4\,\rho_3)}{16\,\rho_1}} \\ &\text{Consequently,} \\ &Y=\pm\sqrt{\frac{\sqrt{(\rho_1^2-4\,\rho_3)^2+8\,\rho_1\rho_2^2}+(\rho_1^2-4\,\rho_3)}{16\,\rho_1}} \\ &Z=\sqrt{\frac{\rho_1}{2}-\frac{\rho_1^2-4\,\rho_3}{8}} \end{aligned}\right\} \tag{45}$$

From the above analysis, the solution of the characteristic equation (39) can approximately be expressed as follows:

$$\left.\begin{aligned} &s_{1,2}=\alpha_1\pm j2\pi f_1=X-\frac{A}{4}\pm j(Y-Z) \\ &s_{3,4}=\alpha_2\pm j2\pi f_2=-X-\frac{A}{4}\pm j(Y+Z) \end{aligned}\right\} \tag{46}$$

The relation between the real part α, the chatter frequency f and the cutting edge setting angle θ is calculated by the system $r=1.5$, using Eq. (46), and is shown in Figs. 31, 32. Fig. 31 shows the case when $\phi=22.5°$, and Fig. 32 shows

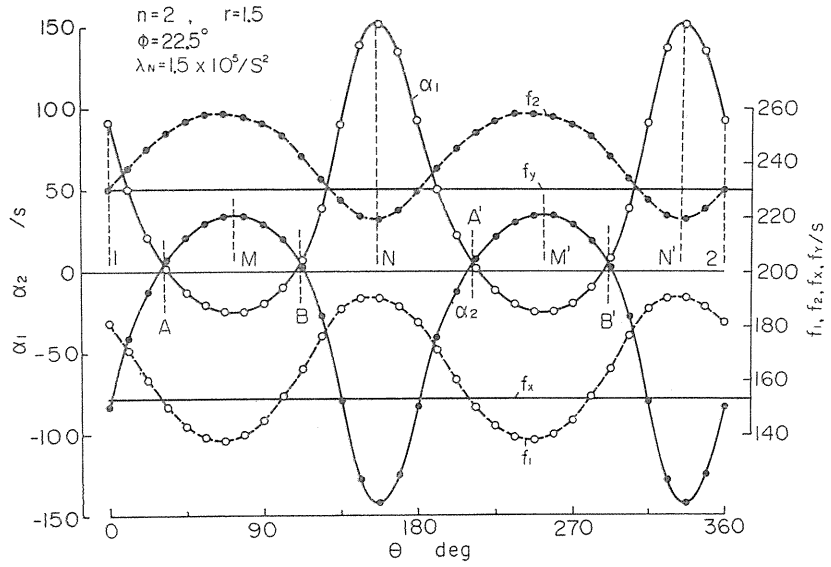

FIG. 31. Variation of increments or decrements α_1, α_2 and frequencies f_1, f_2 with change of cutting edge setting angle θ ($\phi=22.5°$, $r=1.5$).

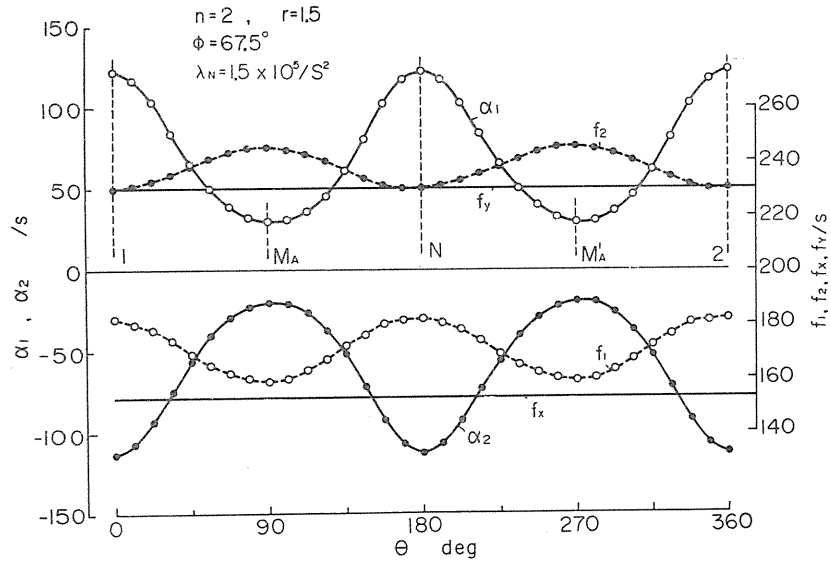

FIG. 32. Variation of increments or decrements α_1, α_2 and frequencies f_1, f_2 with change of cutting edge setting angle θ ($\phi=67.5°$, $r=1.5$).

the case when $\phi=67.5°$. Both figures correspond to the case when $\lambda_N>(\lambda_N)_c$ for all setting angles. In these figures, solid lines indicate the real parts α_1, α_2 and broken lines indicate the chatter frequency f_1, f_2 corresponding to α_1, α_2 respectively. Two straight lines are the two natural frequencies $f_x=p_x/2\pi$, $f_y=p_y/2\pi$.

It is seen in Fig. 31 ($\phi=22.5°$) that either α_1 or α_2 is positive in all setting

angles θ, and the system is unstable for the whole range. In the range 1–A, B–N and B'–2, the vibration occurs with frequency f_1, and within the range A–M–B, A'–M'–B', with f_2. At the intersecting points of the α_1-curve with α_2-curve, vibration with frequencies f_1 and f_2 becomes unstable simultaneously.

It may be quite interesting to compare Fig. 31 with the $r=1.5$ curve in Fig. 21. The fact that α_1 or α_2 becomes maximum at M, M'; N, N' in Fig. 31 corresponds to the fact that the value of $(\lambda_N)_c$ becomes minimum at M, N in Fig. 21. Furtheremore, the values of α_1, α_2 becomes almost zero at A, A'; B, B', and the magnitudes of α_1 and α_2 are reversed at these points. This fact is closely related with $(\lambda_N)_c$ becoming maximum at A, A'; B, B' and decreasing abruptly when passing through these points.

Next, it is seen in Fig. 32 ($\phi=67.5°$) that $\alpha_2<0<\alpha_1$ for all setting angles θ, and vibration occurs with frequency f_1 for whole range. The fact that the value of α_1 becomes minimum at M_A, M'_A corresponds to the results that $(\lambda_N)_c$ becomes maximum at M_A, M'_A in Fig. 23, and the value of $(\lambda_N)_c$ decreases smoothly.

From the above discussion, it is clear that two modes of vibration, that is, f_1 and f_2, satisfy the stability boundary simultaneously and all of the real parts of the characteristic roots become zero at the maximum points of $(\lambda_N)_c$, when $(\lambda_N)_c$ has four maximum values, as seen in Fig. 20 ($\phi=0°$). Hence, $X=A_1/4=0$ in Eq. (46) and the following relation can be obtained

$$\sin(2\theta+\theta_c)=\kappa/\sigma \tag{47}$$

where

$$\left.\begin{aligned}
&\kappa=4n_xp_xH(q+r^2)+2n_x(1+q)\{2n_x(1+q)-p_x^2H(1+r^2)\}\\
&\qquad-4n_x^2p_x(1+q)^2(1+\tau^2\varepsilon)\sin^2\phi\\
&\sigma=n_xH(1+q)\cos\phi\sqrt{\{\tau p\varepsilon_x^2H(r^2-1)-2n_x(q-1)\}^2+\{p_x^2H(r^2-1)-2n_x(q-1)\}^2}\\
&r=p_y/p_x,\quad q=n_y/n_x\\
&\tan\theta_c=\frac{(H_x^2p-2n_x)\cos\phi+\tau(p_x^2h-2n_x)\sin\phi}{(p_x^2H-2n_x)\sin\phi-\tau(p_x^2h-2n_x)\cos\phi}
\end{aligned}\right\} \tag{48}$$

When the condition that $|\kappa/\sigma|\leqq1$ is satisfied, four setting angles θ_{opt} where the value of $(\lambda_N)_c$ becomes maximum can be obtained using Eq. (47) (See Fig. 20). These values of κ, σ are closely related to the vibrational properties of the system, the cutting conditions and the cutting edge setting conditions, as seen in Eqs. (47), (48). Namely, whether four values of θ_{opt} exist or not is determined by these conditions.

Fig. 33 shows the relation for $r=1.5$ tool system between $\sin(2\theta+\theta_c)$, θ_{opt} and ϕ, obtained from Eq. (47). It is seen in the figure that $|\sin(2\theta+\theta_c)|=|\kappa/\sigma|\leqq1$ for ϕ within the range A–B, C–D, and two modes of vibration, that is, f_1 and f_2, become unstable simultaneously at four cutting edge setting angles, that is, $(\theta_1)_{opt}$ and $(\theta_2)_{opt}$. On the contrary, $|\sin(2\theta+\theta_y)|>1$ for ϕ within the range B–C, and there are no cutting edge setting angles that make two modes of vibration unstable simultaneously. So, it is clear that θ_{opt} is not found in four cutting edge setting angles. These facts correspond to the considerations in Figs. 20~24 closely.

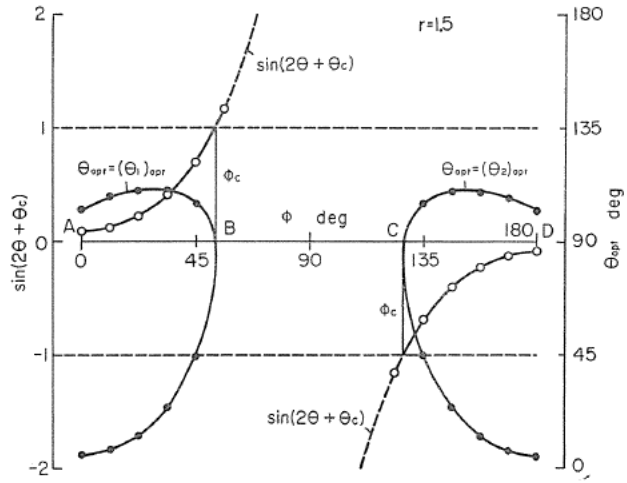

FIG. 33. Relation between $\sin(2\theta+\theta_c)$, optimum cutting edge setting angle θ_{opt} and shifted angle ϕ ($r=1.5$).

As seen in Figs. 20~24, $(\lambda_N)_c$-curves change smoothly for the cutting edge setting angles near θ_{opt}, when $(\lambda_N)_c$ has two maximum values. Consequently, it is convenient for practical application that the value of $(\lambda_N)_c$ is not so much affected by the small error in cutting edge setting angle from θ_{opt}.

Next, to make clear the effect of the vibrational properties of the system and cutting conditions on the number (four or two) of the maximum values of $(\lambda_N)_c$, the critical shifted angle ϕ_c for which Eq. (47) has a solution is calculated for the $r=1.1$, $r=1.5$ systems, and is shown in Figs. 34 and 35. Fig. 34 shows the relation between ϕ_c and the damping coefficient n_x. The value of n_x is determined by the relation that $n \propto p^2$ (See Fig. 19). It is seen in the figure that ϕ_c decreases with increase of n_x, hence the range of ϕ where $(\lambda_N)_c$ has four maximum values for both systems narrows. This tendency is conspicuous in fhe system of large frequency ratio r.

Next, Fig. 35 shows the relation between ϕ_c and τ. It may be noted in the figure that the greater the ratio τ is, and for the same magnitude of τ the greater

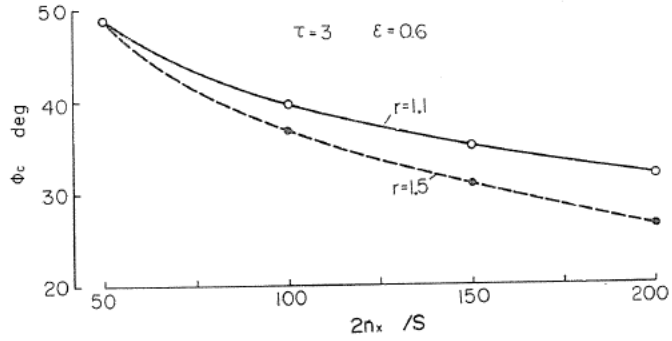

FIG. 34. Relation between critical shifted angle ϕ_c and damping coefficient n_x ($r=1.1$, $r=1.5$).

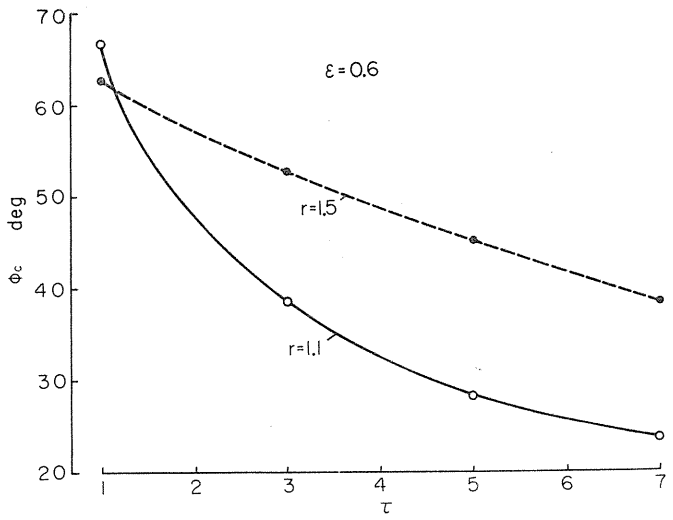

FIG. 35. Relation between critical shifted angle ϕ_c and ratio τ ($r=1.1$, $r=1.5$).

the ratio r is, the greater the value of ϕ_c is, hence, the range in which $(\lambda_N)_c$ has four maximum values is broad.

3.2. Experimental result

To ascertain the above theoretical analysis, the following experiments are carried out. Four cutting tools having different amounts of directional characteristics are made (See Fig. 17 and Table 2) and two equal dimensioned cutting edges (rake angle: 0°, side clearance angle: 6°, nose radius: 0.5 mm) are set to each cutting tool. Boring operation is carried out in such cutting conditions that the cutting velocity is about 15 m/min, the feed rate is 0.1 mm/rev which is held constant, the cutting factors of both cutting edges are equal, *i.e.*, $g_1=g_2=1$ and depth of cut is changed for various cutting edge setting angles, and the critical depth of cut at which the chatter vibration is set up is examined experimentally. The vibrations of x and y directions are measured electrically by the strain gauges. Fig. 36 shows an example of chatter vibration in both x and y directions for the $r=1.5$ tool system.

Figs. 37~39 show some examples of the relations between the amplitude of the chatter and the depth of cut obtained from many experimental photographs for $r=1.5$. From the amplitude-depth of cut curves in the figures, the critical depth of cut d_c can be obtained experimentally for various cutting edge setting angles. Here, it must be noted that the critical depth of cut d_c is equivalent to $(\lambda_N)_c$ in the theoretical analysis.

Figs. 40~43 show the relations between d_c and θ for $r=1.5$ tool system. The calculated value $(\lambda_N)_c$ is illustrated by solid line in the figures, for reference. Figs. 40, 41 are the results for $\phi=0°$, 180° and $\phi=45°$, 135° where the stability boundary $(\lambda_N)_c$ becomes maximum in four cutting edge setting angles. Fig. 42 is the result for $\phi=67.5°$, 112.5° where $(\lambda_N)_c$ becomes maximum at two angles. Fig. 43 shows the case of $\phi=90°$ where two cutting edges are set vertically to

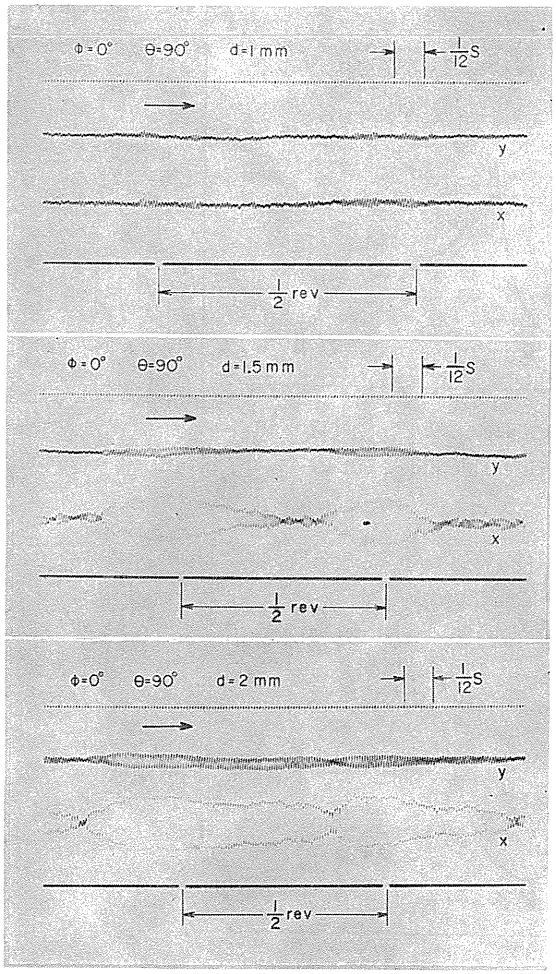

FIG. 36. Experimental records of chatter vibration ($r=1.5$).

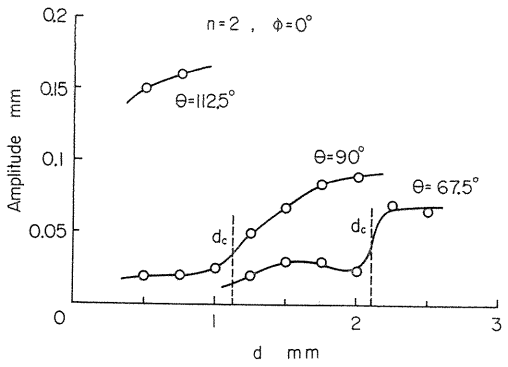

FIG. 37. Variation of amplitude with change of depth of cut d for various cutting edge setting angles ($\phi=0°$).

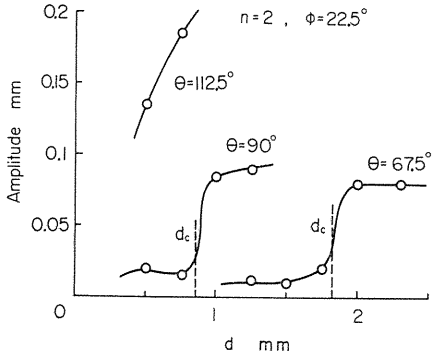

FIG. 38. Variation of amplitude with change of depth of cut d for various cutting edge setting angles ($\phi=22.5°$).

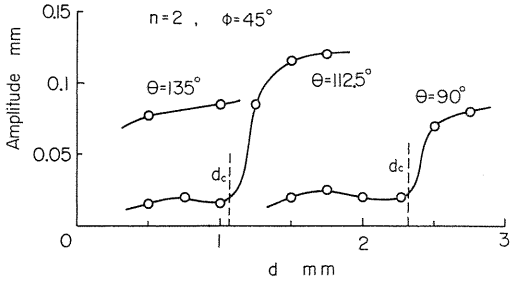

FIG. 39. Variation of amplitude with change of depth of cut d for various cutting edge setting angles ($\phi=45°$).

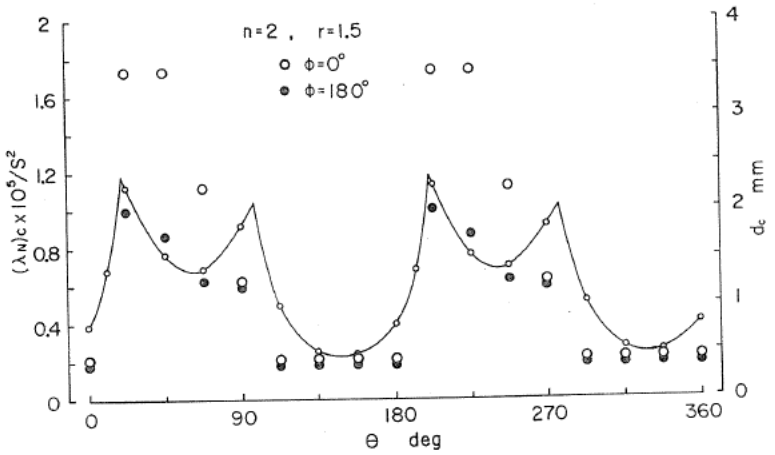

FIG. 40. Experimental result of critical depth of cut d_c ($\phi=0°$, 180°).

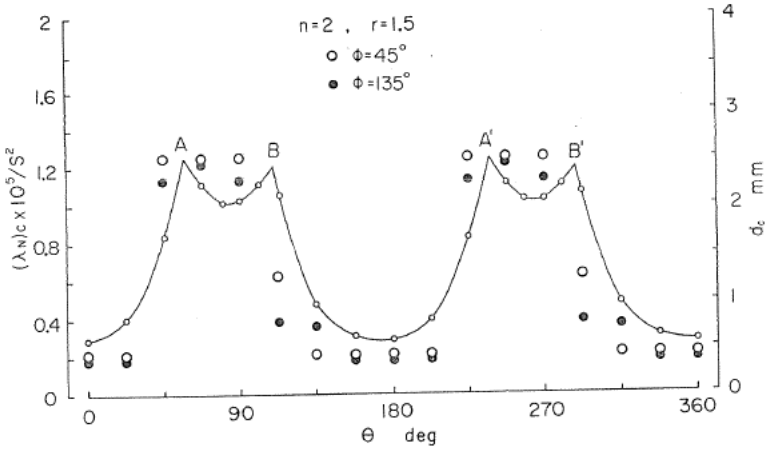

FIG. 41. Experimental result of critical depth of cut d_c ($\phi=45°$, 135°).

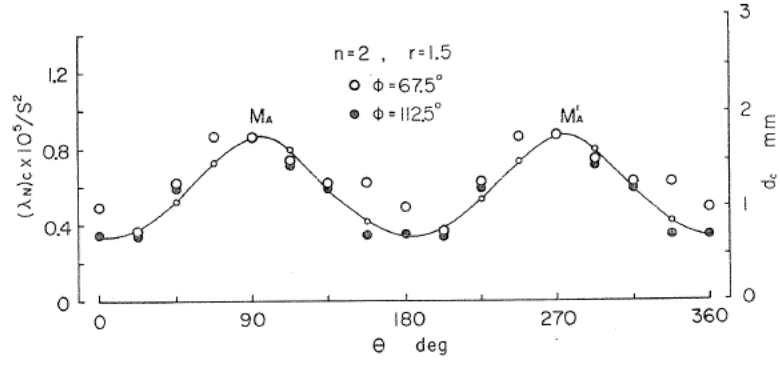

FIG. 42. Experimental result of critical depth of cut d_c ($\phi=67.5°$, 112.5°).

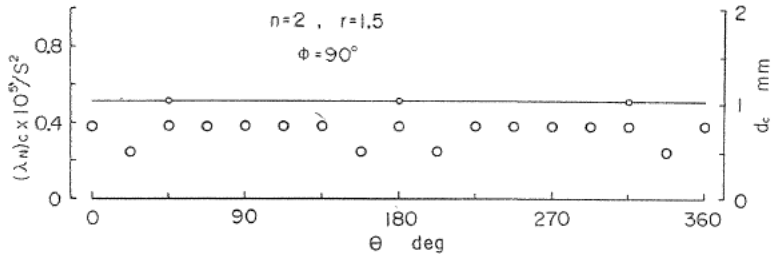

FIG. 43. Experimental result of critical depth of cut d_c ($\phi=90°$).

each other, and $(\lambda_N)_c$ is independent of θ, regardless of the presence of the directional characteristics in the vibrational properties. It is clear in Figs. 40~43 that the experimental results show a closely similar tendency to the theoretical results. Consequently, it is ascertained that the analytical results are in good agreements with the experimental results quantitatively.

3.3. Conclusion

The stability boundary for the chatter vibration occurring in the multi-edge rotary cutting tool which has the directional characteristics in the vibrational properties is introduced as the function of the vibrational properties of the system and the cutting conditions, and is ascertained experimentally.

As a result, it has been shown that the chatter vibration of the multi-edge rotary cutting tool can remarkably be prevented through a good use of the directional characteristics of the system and a proper combination of the setting angle of each cutting edge. Furthermore, it has been shown that there is the optimum tool configuration to prevent the chatter vibration, and this optimum tool configuration has no relation with the cutting conditions and the cutting edge setting angles.

4. Some Considerations on Prevention of Chatter Vibration in Multi-edge Rotary Cutting Tool, 2[12)13)]

In the previous chapter, the stability boundary of chatter occurring in the multi-edge rotary cutting tools which had a directional characteristics in the vibrational properties was introduced theoretically as the functions of the vibrational properties of the system and the various cutting conditions, and was ascertained experimentally.

In this chapter, based on the analytical results in the previous chapter, the effects of the cutting edge setting condilions in axial or radial directions and small errors in the cutting edge setting conditions (such as cutting angle, nose radius etc.) on the stability boundary are examined from a practical point of view.

4.1. Tools with two cutting edges ($n=2$)

In the previous chapter, only the stability boundary in the case that all of the cutting factors are equal, that is, $g_i=1$ [See Eq. (35)] was treated.

The cutting factor g_i is generally determined by the geometrical setting conditions and the dimensions of each cutting edge. For example, Fig. 44 shows the relation between g_i and the setting conditions of each cutting edge, for the

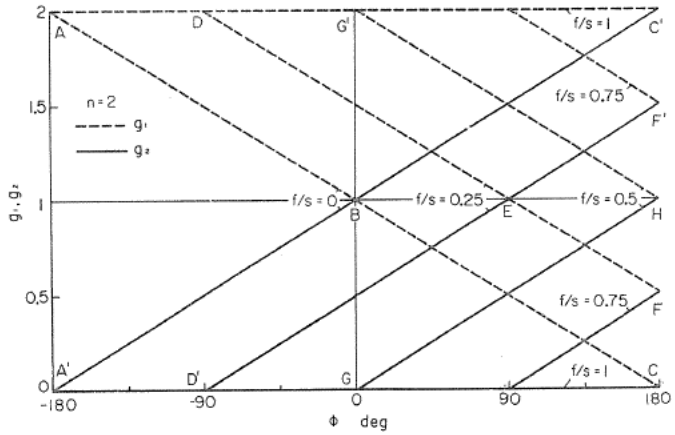

FIG. 44. Relation between cutting factor g_i and cutting edge setting condition ($n=2$).

tool with two cutting edges having equal dimensions ($n=2$). As seen in Eq. (35), $g_1+g_2=2$ for the case that $n=2$. In the figure, f/s is a parameter indicating the ratio of the setting error in axial direction f to the feed rate per revolution s, ϕ indicates the shifted angle from the symmetrical direction of both cutting edges as shown in Fig. 45. When $f/s=0.25$, g_1 shows the changing process of A–D–E–F and g_2 shows that of A'–D'–E–F' with increase of the shifted angle ϕ, as shown in the figure. Namely, $g_1=2$, $g_2=0$ for the case that $-180°<\phi<-90°$, hence, cutting edge C_2 does not contribute to metal removing at all.

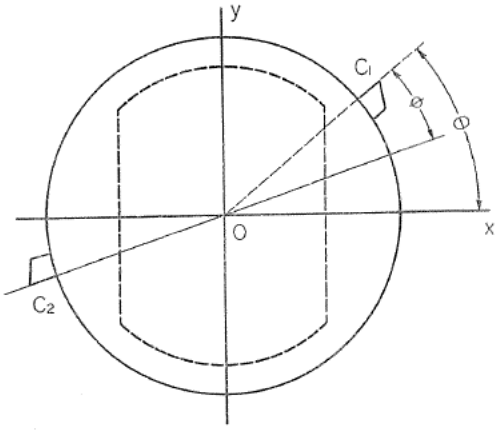

FIG. 45. Cutting edge setting angle ($n=2$).

And for the greater shifted angle, g_1 decreases and g_2 increases, hence, both cutting edges C_1, C_2 contribute to metal removing. Particularly, in the case of $\phi=90°$, $g_1=g_2=1$, that is, the contributing rates of both cutting edges are equal. Furthermore, it is seen in the figure that when $f/s=1$, $g_1=2$ and $g_2=0$ for arbitrary shifted angle ϕ, hence, cutting edge C_2 does not contribute to metal removing. Symmetrical setting condition of the two cutting edges corresponds to the point B ($\phi=0°$, $f/s=0$) in the figure.

It may be considered that the stability boundary of the chatter vibration is affected by accidental or intentional changes of each cutting edge setting condition in this manner. On that account, the effect of the various cutting edge setting conditions on the stability boundary of multi-edge rotary cutting tools will be examined from a practical point of view.

4.1.1. Effect of g_i ($n=2$)

First, to make clear the relation between the stability boundary $(\lambda_N)_c$ and the

cutting factor g_i, the stability boundary $(\lambda_N)_c$ is calculated for the actual tool system used in the previous chapter, varing the value of g_i. Figs. 46~49 show examples of these calculations. In the calculations, the following numerical values are used, $H=0.0005$ sec, $\varepsilon=h/H=0.6$, $\tau=3$.

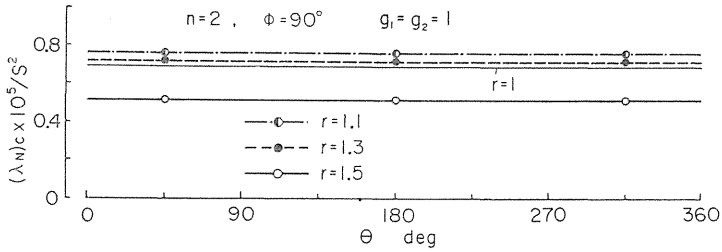

FIG. 46. Variation of stability boundary $(\lambda_N)_c$ with change of cutting edge setting angle θ ($\phi=90°$, $g_1=1$).

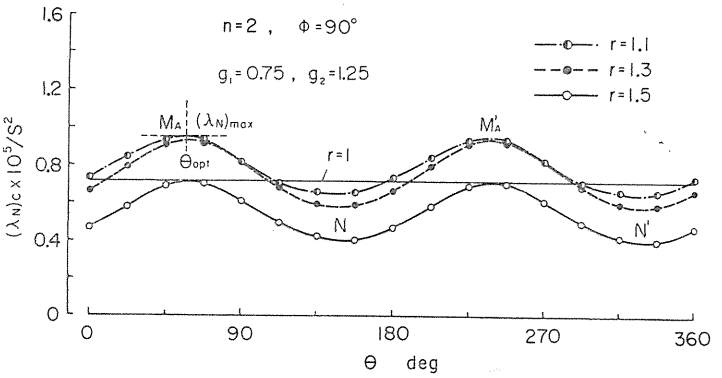

FIG. 47. Variation of stability boundary $(\lambda_N)_c$ with change of cutting edge setting angle θ ($\phi=90°$, $g_1=0.75$).

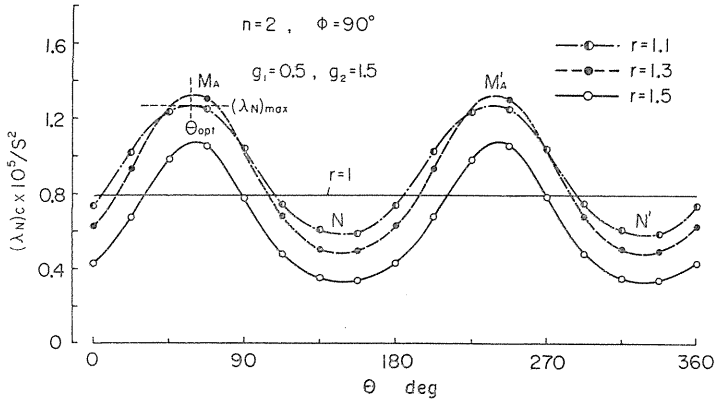

FIG. 48. Variation of stability boundary $(\lambda_N)_c$ with change of cutting edge setting angle θ ($\phi=90°$, $g_1=0.5$).

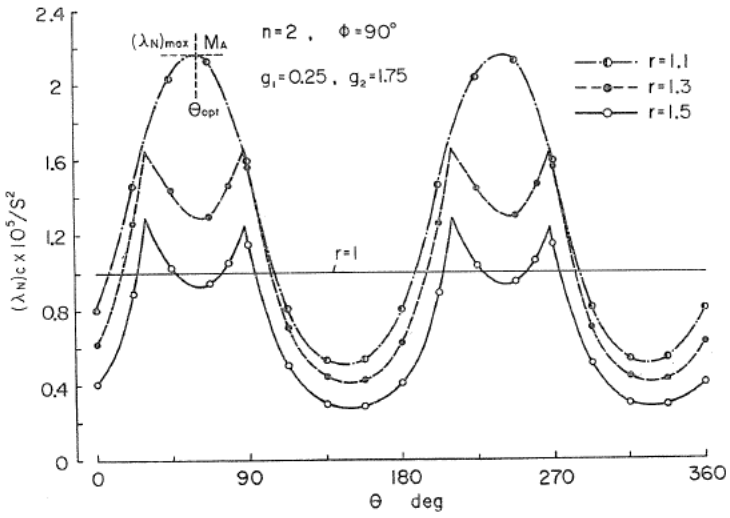

FIG. 49. Variation of stability boundary $(\lambda_N)_c$ with change of cutting edge setting angle θ ($\phi=90°$, $g_1=0.25$).

Figs. 46~49 show the relations between the stability boundary $(\lambda_N)_c$ and the cutting edge setting angle θ for the case of $\phi=90°$ (See Fig. 45) where both cutting edges lie in a rectangular position to each other, and the values of g_1 are 1.0, 0.75, 0.5, 0.25 respectively (hence, the corresponding values of g_2 are 1.0, 1.25, 1.5, 1.75). In the case of $\phi=90°$, $g_1=g_2=1$, as shown in Fig. 46, the stability boundary $(\lambda_N)_c$ is independent of the cutting edge setting angle θ, regardless of the presence of the directional characteristics in the vibrational properties. On the contrary, it is seen in Figs. 47~49 where the value of g_1 is varied that $(\lambda_N)_c$ is markedly influenced by the cutting edge setting angle θ, that is to say, when $g_1=0.75$, 0.5, $(\lambda_N)_c$ has four maximum values in some cases ($r=1.3$, 1.5). And these maximum values are fairly greater than the stability boundary $(\lambda_N)_c$ of the $r=1$ tool system as a rule.

Fig. 50 shows the relation between the maximum value $(\lambda_N)_{max}$ and the cutting factor g_1, which is obtained from the above calculaitons ($\phi=90°$). In the figure, the range A–B corresponds to the case where $(\lambda_N)_c$ has four maximum values, and the range B–C corresponds to the case where $(\lambda_N)_c$ has two maximum values. It is recognized in Fig. 50 that the value of $(\lambda_N)_{max}$ becomes maximum and the chatter vibration can most effectively be prevented in $0<g_1<0.25$ for $r=1.1$ tool system, and for $r=1.3$, $r=1.5$ tool systems, at the critical point B at which the number of the maximum values of $(\lambda_N)_c$ changes from four to two.

Fig. 51 shows the relation between $(\lambda_N)_{max}$ and g_1 for $\phi=0°$ where two cutting edges are set symmetrically. In the case of $\phi=0°$, $g_1=g_2=1$, $(\lambda_N)_c$ has four maximum values, as shown in Fig. 20 of the previous chapter. The maximum value $(\lambda_N)_{max}$ is not affected by the change of g_1 when $\phi=0°$, as shown in Fig. 51. Accordingly, the setting errors in axial or radial direction, which happen accidentally or intentionally, do not affect the chatter vibration when $\phi=0°$.

In the above considerations, the effect of g_1 on the chatter prevention is examined only for $\phi=90°$, 0°. It is understood, however, from the above discussion

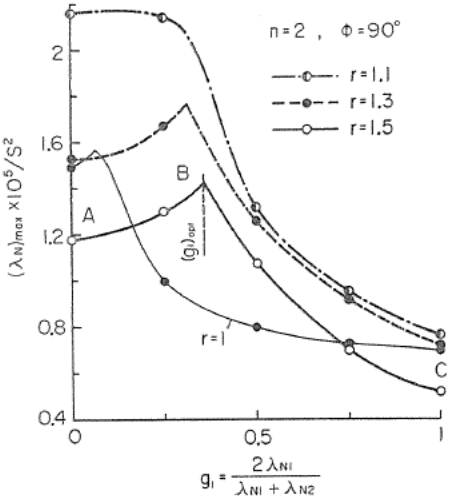

FIG. 50. Relation between maximum value $(\lambda_N)_{max}$ and cutting factor g_1 (ϕ= 90°).

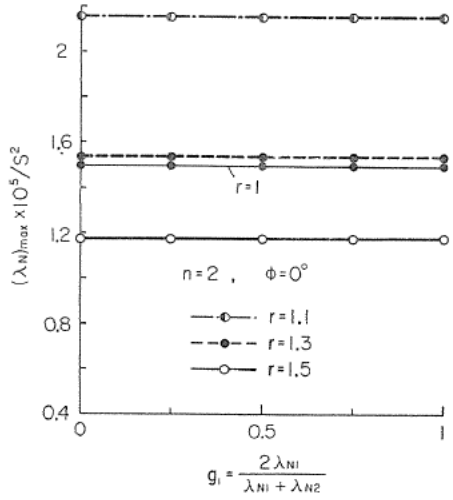

FIG. 51. Relation between maximum value $(\lambda_N)_{max}$ and cutting factor g_1 (ϕ= 0°).

that the cutting factor g_i has a great influence on the stability boundary of the chatter vibration, and the degree of influence varies remarkably with the shifted angle ϕ.

4.1.2. Effect of ϕ (n=2)

It is ordinary in common multi-edge rotary cutting tools that all of the cutting edges are set in the concyclic position, owing to the structure of the tools. In this case, provided that all of the cutting edge dimensions are equal, then $g_1=g_2=1$. As a matter of fact, it is shown in the previous chapter that the chatter behaviour will be remarkably improved by the unsymmetrical setting condition of each cutting edge.

In the case of the concyclic setting of two cutting edges, if one of the cutting edges is shifted from the symmetrical setting condition as shown in Fig. 45, the variational configuration of $(\lambda_N)_c$ is influenced not only by the shifted angle ϕ, but also by the dependent change of the cutting factor g_1, g_2. Provided that two cutting edges have the same dimension, then g_1, g_2 are shown as a function of the shifted angle ϕ as follows:

$$\left.\begin{aligned} g_1 &= 1-\phi/180 \\ g_2 &= 1+\phi/180 \end{aligned}\right\} \tag{49}$$

Figs. 52~55 show the variation of the stability boundary $(\lambda_N)_c$ with the change of the cutting edge setting angle θ for various shifted angles ϕ of the two cutting edges which are set in concyclic positions.

Fig. 52 shows the case of $\phi=0°$, that is, two cutting edges are set symmetrically. In this case, $g_1=g_2=1$, so the figure is identical with Fig. 20. However, comparing Figs. 53~55 with the corresponding Figs. 22, 24 of the previous chapter (in which $g_1=g_2=1$), it becomes clear that there is a wide difference in the vari-

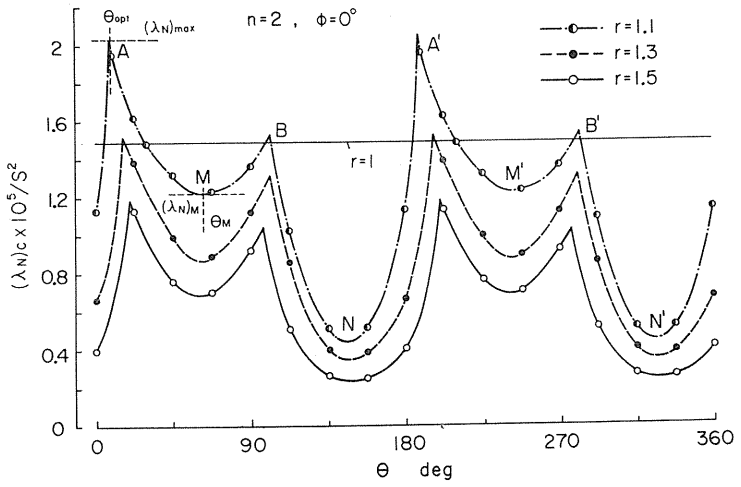

FIG. 52. Variation of stability boundary $(\lambda_N)_c$ with change of cutting edge setting angle $\theta(\phi=0°)$.

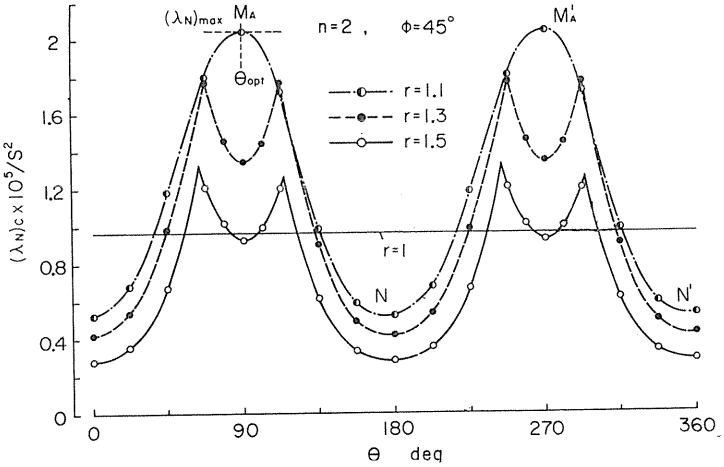

FIG. 53. Variation of stability boundary $(\lambda_N)_c$ with change of cutting edge setting angle θ $(\phi=45°)$.

ational configuration of $(\lambda_N)_c$ and the corresponding maximum value $(\lambda)_{max}$. Namely, comparing Fig. 53 $(\phi=45°)$ with Fig. 22 $(\phi=45°, g_1=g_2=1)$, it is recognized that the variational configurations of both cases is identical, however, there is a wide difference in the corresponding maximum values $(\lambda_N)_{max}$. Next, on the case of $\phi=90°$, $g_1=g_2=1$, the stability boundary $(\lambda_N)_c$ is independent of the cutting edge setting angle θ, regardless of the presence of the directional characteristics in the vibrational properties, however, in the case of concyclic setting conditions $(\lambda_N)_c$ has two maximum values and there exist the optimum cutting edge setting angles θ_{opt}. In the case of $\phi=135°$, $g_1=g_2=1$, the variational configuration of $(\lambda_N)_c$ agrees with that of $\phi=45°$ and $g_1=g_2=1$, and $(\lambda_N)_c$ has two optimum cutting

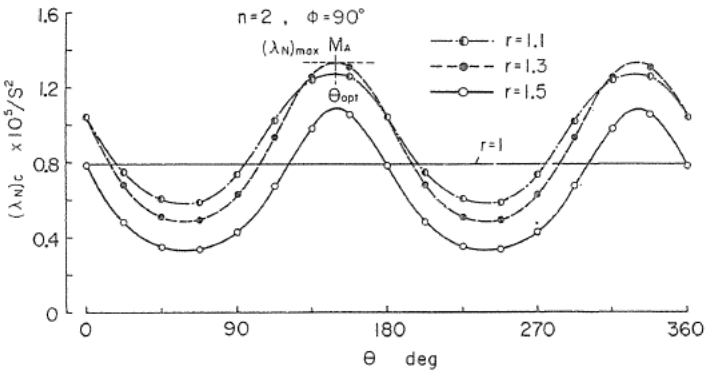

FIG. 54. Variation of stability boundary $(\lambda_N)_c$ with change of cutting edge setting angle θ ($\phi=90°$).

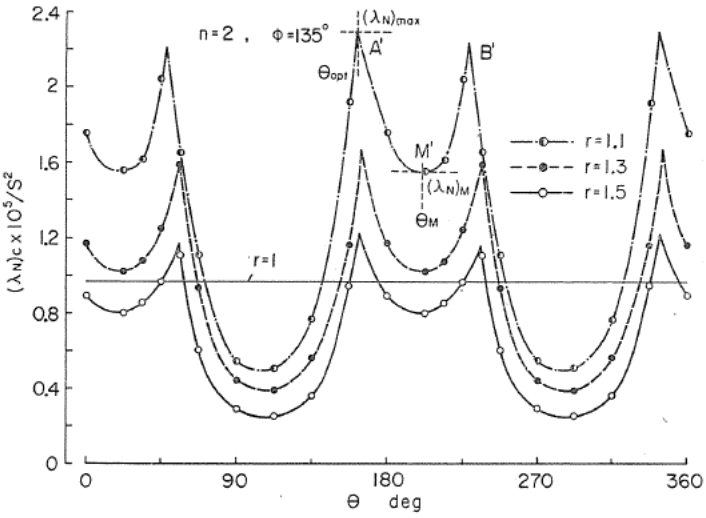

FIG. 55. Variation of stability boundary $(\lambda_N)_c$ with change of cutting edge setting angle θ ($\phi=135°$).

edge setting angles (See Fig. 22). On the contrary, in the case of concyclic setting condition, the value of $(\lambda_N)_c$ becomes maximum at four cutting edge setting angles. These differences are caused by the change of g_1 depending on the change of ϕ.

Accordingly, comparing Figs. 56, 57, showing the relations between the maximum value $(\lambda_N)_{max}$, the optimum cutting edge setting angle θ_{opt} and the shifted angle ϕ, with the corresponding Figs. 25, 26 in the previous chapter, it is recognized that the values of $(\lambda_N)_{max}$ and θ_{opt} are different from each other by r and ϕ. Namely, in the case of $g_1=g_2=1$, the variational configuration of $(\lambda_N)_{max}$ has the tendency of line symmetry at $\phi=90°$ and $\phi=-90°$, and $(\lambda_N)_{max}$ becomes maximum at $\phi=0°$, $\phi=180°$ for the $r=1.1$ tool system, and at four setting directions B, C, D, E for the $r=1.3$, 1.5 tool systems. On the contrary, in the case of the concyclic

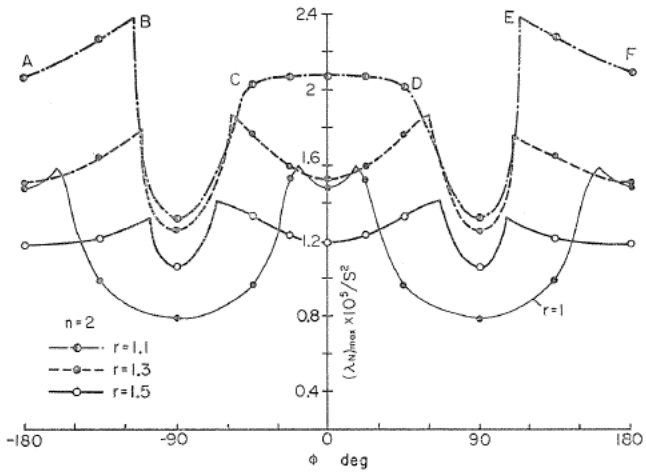

FIG. 56. Relation between maximum value $(\lambda_N)_{max}$ and shifted angle ϕ $(n=2)$.

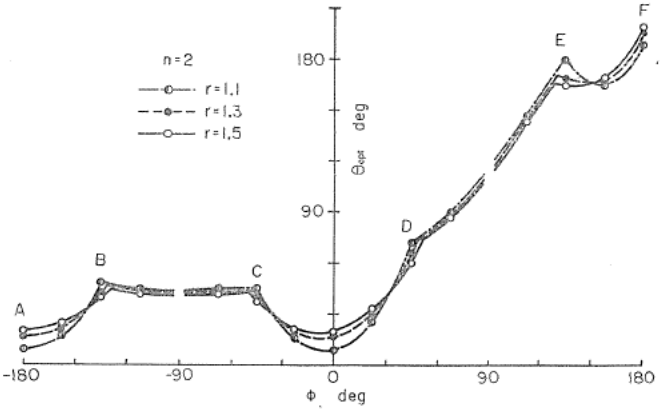

FIG. 57. Relation between optimum cutting edge setting angle θ_{opt} and shifted angle ϕ $(n=2)$.

setting conditions, this tendency of line symmetry is not recognized and $(\lambda_N)_{max}$ becomes maximum at two setting directions B, E for the $r=1.1$ tool system and at C, D for the $r=1.3$, $r=1.5$ tool systems.

From the above discussion, it is clear that the chatter vibration of the multi-edge rotary cutting tool can be prevented through a good use of the directional characteristics of the system and a proper combination of the setting angle of each cutting edge in the case of concyclic setting condition, too.

4.1.3. Effect of small change in g, ϕ on stability boundary $(n=2)$

It is ordinary in common multi-edge rotary cutting tools that all of the cutting edges are set symmetrically, that is, $\phi=0°$, $g_i=1$. However, it may be inevitable that small changes in g_i or ϕ are apt to occur owing to the setting error or the

error in tool dimension, produced by the tool forming or tool wear.

Therefore, the effect of a small change in g or ϕ on the stability boundary will be examined.

Expanding Eq. (40) into a polynomial of λ_N and using Eqs. (38), (39), a fifth degree polynomial equation for λ_N is obtained as follows:

$$a(g_i, \phi)\lambda_N^5 + b(g_i, \phi)\lambda_N^4 + c(g_i, \phi)\lambda_N^3 + d(g_i, \phi)\lambda_N^2 + e(g_i, \phi)\lambda_N + f = 0 \qquad (50)$$

where $a(g_i, \phi)$, $b(g_i, \phi)$, $c(g_i, \phi)$, $d(g_i, \phi)$ and $e(g_i, \phi)$ are the functions of cutting edge setting conditions g_i, ϕ; and f is a constant free from g_i and ϕ.

Differentiating Eq. (50) by g_i or ϕ, then

$$\frac{\partial \lambda_N}{\partial z} = -\left\{\frac{\partial a(g_i, \phi)}{\partial z}\lambda_N^5 + \frac{\partial b(g_i, \phi)}{\partial z}\lambda_N^4 + \frac{\partial c(g_i, \phi)}{\partial z}\lambda_N^3 + \frac{\partial d(g_i, \phi)}{\partial z}\lambda_N^2 + \frac{\partial e(g_i, \phi)}{\partial z}\lambda_N\right\} \Big/ \{5a(g_i, \phi)\lambda_N^4 + 4b(g_i, \phi)\lambda_N^3 + 3c(g_i, \phi)\lambda_N^2 + 2d(g_i, \phi)\lambda_N + e(g_i, \phi)\} \qquad (51)$$

where $z = g_i$ or $z = \phi$.

Substituting the stability boundary $(\lambda_N)_c$ into Eq. (51), $\partial(\lambda_N)_c/\partial g_1$, $\partial(\lambda_N)_c/\partial\phi$ are given. These differential cofficients represent the effect of a small change in g, ϕ on the stability boundary $(\lambda_N)_c$.

Figs. 58, 59 show the variation of the differential coefficients $\partial(\lambda_N)_c/\partial g_1$, $\partial(\lambda_N)_c/\partial\phi$ with the change of the cutting edge setting angle θ for the $r=1.5$ tool system, using the above mentioned method. The stability boundary $(\lambda_N)_c$ is illustrated by the broken line in the figure, for reference.

Fig. 58 shows a symmetrical setting of two cutting edges ($\phi=0°$). It is seen in the figure that the value of $\partial(\lambda_N)_c/\partial\phi$ varies according to the cutting edge setting angle θ, and $\partial(\lambda_N)_c/\partial\phi$ becomes maximum only in the neighbourhood of the optimum cutting edge setting angle θ_{opt} where $(\lambda_N)_c$ becomes maximum. This is a very convenient fact to prevent the chatter vibration. The value of $(\lambda_N)_c$ at A (first order of θ_{opt}) is slightly greater than that at B (second order of θ_{opt}); contrast with this fact the value of $\partial(\lambda_N)_c/\partial\phi$ at B is greater than that at A. Because of this, which θ_{opt} (first order or second order) is to be selected must be determined in due consideration of the practical problem in tool forming and setting. On the contrary, $\partial(\lambda_N)_c/\partial g_1 = 0$ for all cutting edge setting angles θ, hence, a setting error of the cutting edges in the axial direction does not influence the stability boundary $(\lambda_N)_c$ at all.

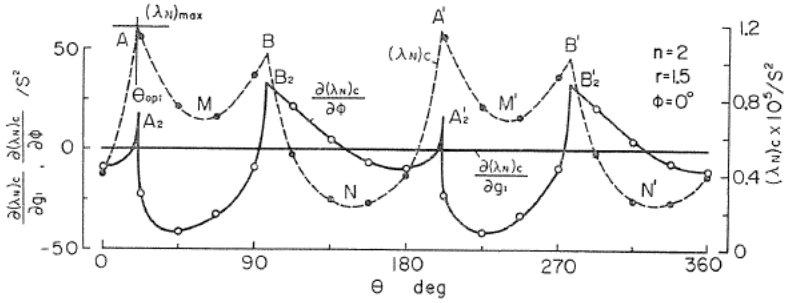

FIG. 58. Variation of differential coefficients $\partial(\lambda_N)_c/\partial g_1$, $\partial(\lambda_N)_c/\partial\phi$ and stability boundary $(\lambda_N)_c$ with change of cutting edge setting angle θ ($n=2$, $\phi=0°$).

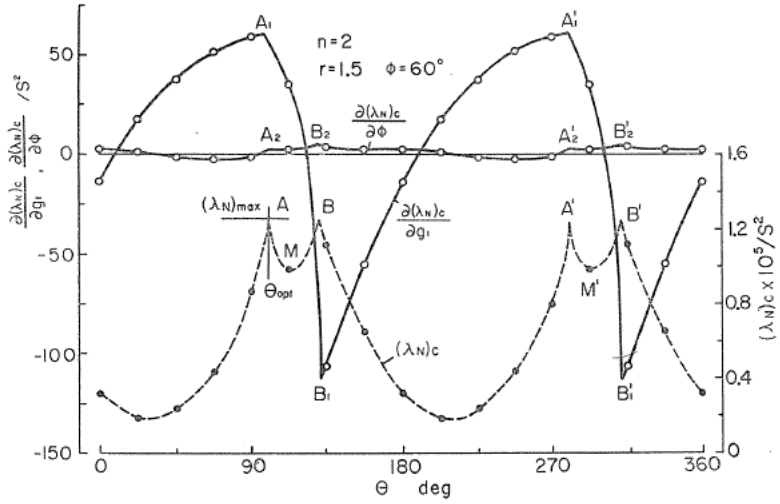

FIG. 59. Variation of differential coefficients $\partial(\lambda_N)_c/\partial g_1$, $\partial(\lambda_N)_c/\partial\phi$ and stability boundary $(\lambda_N)_c$ with change of cutting edge setting angle θ ($n=2$, $\phi=60°$).

Next, Fig. 59 shows the case of $\phi=60°$, and in this setting conditin $(\lambda_N)_{max}$ becomes maximum and the chatter vibration can most effectively be prevented, as seen in Fig. 56. In this case, both small changes of g and ϕ affect the stability boundary $(\lambda_N)_c$. That is, $\partial(\lambda_N)_c/\partial g_1>0$ at the first order of θ_{opt} (A, A'), and $\partial(\lambda_N)_c/\partial g_1<0$ at the second order of θ_{opt} (B, B'). Furthermore, $\partial(\lambda_N)_c/\partial\phi>0$ at the first and the second order of θ_{opt}. Considering the above mentioned points and that the maximum values $(\lambda_N)_{max}$ at the first and the second order of θ_{opt} are approximately equal, the first order of θ_{opt} is found good to prevent the chatter vibration for the case of $\phi=60°$.

From the above consideration, it is clear that the optimum cutting edge setting angle must be determined in due consideration of the effect of a small change in g or ϕ on the stability boundary $(\lambda_N)_c$.

4.2. Tools with 3 or 4 cutting edges

In the previous section, the stability boundary of the tools with two cutting edges is studied. The stability boundary with more than three cutting edges can be discussed using the above mentioned method.

4.2.1. Tools with three cutting edges ($n=3$)

4.2.1.1. Effect of ϕ

Many multi-edge rotary cutting tools have generally the cutting edges set in concyclic positions at regular intervals. The stability boundary of the chatter vibration is calculated for the case where one of the three cutting edges is shited from the symmetrical setting condition ($\phi\neq0°$) as shown in Fig. 60, as well as for the symetrical setting condition. In this case, the values of g_i are determined as follows:

$$\left.\begin{aligned} g_1 &= 1+\phi/120 \\ g_2 &= 1 \\ g_3 &= 1-\phi/120 \end{aligned}\right\} \qquad (52)$$

In Fig. 61 where three cutting edges are set in a symmetrical setting condition, the stability boundary $(\lambda_N)_c$ is not affected by the cutting edge setting angle θ, regardless of the presence of the directional characteristics in the vibrational properties, and this tendency is not agreeable with that of $n=2$. Furthermore, the stability boundary $(\lambda_N)_c$ of the tool systems of $r=1.1$ and $r=1.3$ is greater than that of the $r=1$ tool system which has no directional characterics. Next, Fig. 62 is the result for $\phi=67.5°$, where the stability boundary $(\lambda_N)_c$ of the $r=1.1$, 1.3 and 1.5 tool

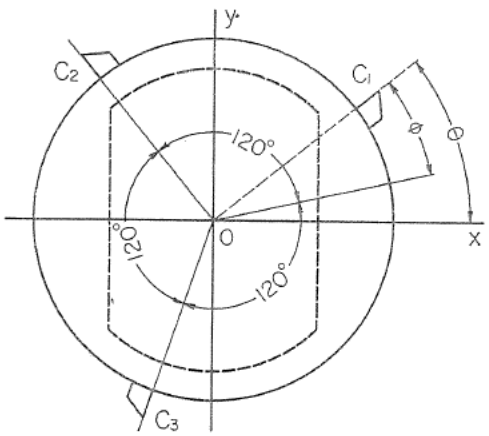

FIG. 60. Cutting edge setting angle ($n=3$).

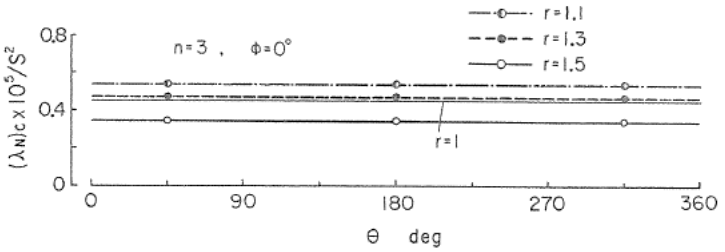

FIG. 61. Variation of stability boundary $(\lambda_N)_c$ with change of cutting edge setting angle θ ($\phi=0°$).

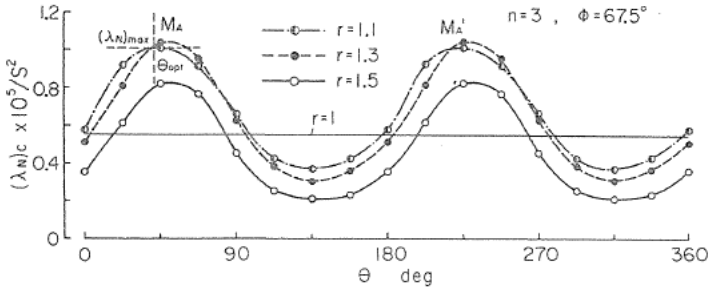

FIG. 62. Variation of stability boundary $(\lambda_N)_c$ with change of cutting edge setting angle θ ($\phi=67.5°$).

systems becomes maximum at two cutting edge setting angles θ_{opt} (M_A, M_A') and these maximum values are considerably greater than the stability boundary $(\lambda_N)_c$ of $r=1$ tool system. Fig. 63 shows the result for $\phi=-67.5°$, where the stability boundary $(\lambda_N)_c$ becomes maximum at four cutting edge setting angles, and this tendency differs from the tendency in Figs. 61, 62. Figs. 64, 65 show the relation between the maximum value $(\lambda_N)_{max}$, the corresponding optimum cutting edge

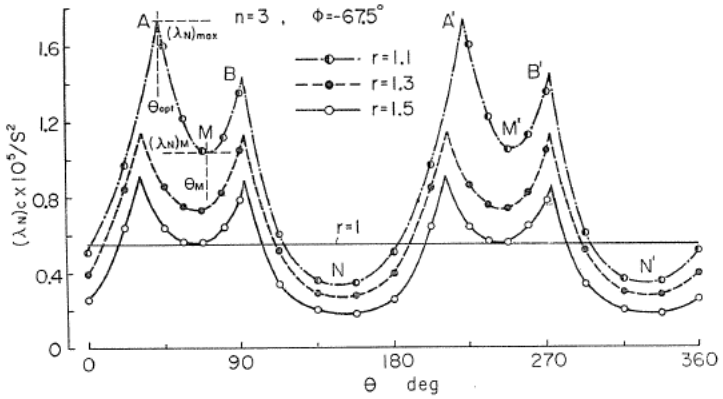

FIG. 63. Variation of stability boundary $(\lambda_N)_c$ with change of cutting edge setting angle θ ($\phi = -67.5°$).

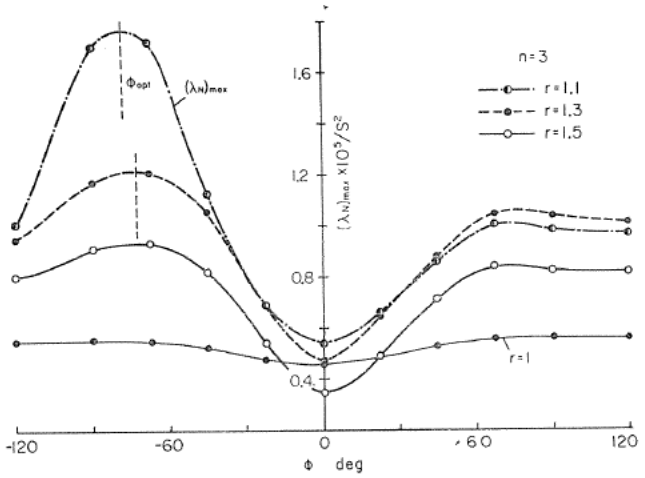

FIG. 64. Relation between maximum value $(\lambda_N)_{max}$ and shifted angle ϕ ($n=3$).

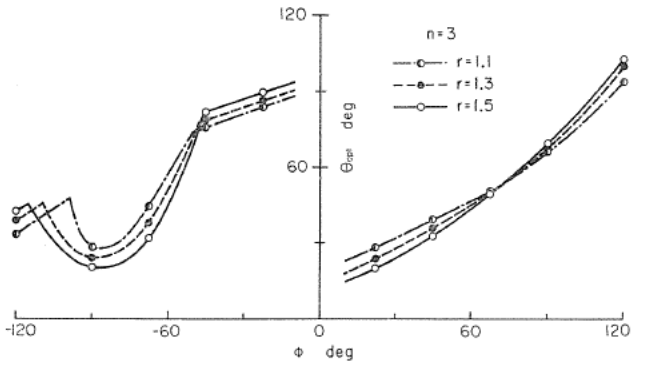

FIG. 65. Relation between optimum cutting edge setting angle θ_{opt} and shifted angle ϕ ($n=3$).

setting angle θ_{opt} and the shifted angle ϕ. It is seen in Fig. 64 that the value of $(\lambda_N)_{max}$ at $\phi=0°$ where three cutting edges are set symmetrically is the smallest, and $(\lambda_N)_{max}$ becomes maximum in the neighborhood of $\phi=-60°$. This maximum value is heavily dependent on the frequency ratio r, that is, on the degree of the directional characteristics in the vibrational properties, and that of the $r=1$ tool system is the smallest of all. In the above discussion, it is expected that the chatter vibration will be remarkably improved by using a proper combination of r, ϕ, θ. However, it must be noted that when $\phi\neq 0°$, the tool displaces owing to the unvalance of cutting forces acting on each cutting edge.

4.2.1.2. Effect of small change in g, ϕ on stability boundary

The effect of a small change in g or ϕ on the stability boundary will be examined for $r=1.5$ tool system.

Fig. 66 shows the variation of the differential coefficients $\partial(\lambda_N)_c/\partial g_1$, $\partial(\lambda_N)_c/\partial\phi$ with the change of the cutting edge setting angle θ for $\phi=0°$, to make clear the effect of a small change in g, ϕ on the stabilility boundary of the chatter vibration. Though the stability boundary $(\lambda_N)_c$ is independent of the cutting edge setting angle θ in case of $\phi=0°$ as shown in Fig. 61, $(\lambda_N)_c$ is influenced by a small error in both g and ϕ. $\partial(\lambda_N)_c/\partial g_1$ becomes maximum at A, A' and $\partial(\lambda_N)_c/\partial\phi$ becomes maximum in D, D'. Hence, these cutting edge setting angles are desiable to prevent the chatter vibration, but the differential coefficients $\partial(\lambda_N)_c/\partial g_1$, $\partial(\lambda_N)_c/\partial\phi$ do not become maximum at the same cutting edge setting angle. In the actual multi-edge rotary cutting tool, it is conceivable that small errors in g and ϕ coexist in many cases. From a practical point of view, it is desired that $\partial(\lambda_N)_c/\partial g_1>0$ and $\partial(\lambda_N)_c/\partial\phi>0$ are simultaneously satisfied. Then, the cutting edge setting angles near the intersecting points of these two curves, θ_1 and θ_2 are desiable for the prevention of the chatter vibration.

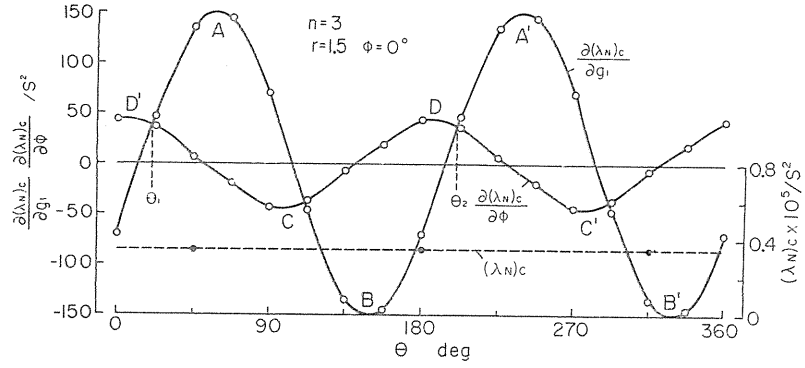

FIG. 66. Variation of differential coefficients $\partial(\lambda_N)_c/\partial g_1$, $\partial(\lambda_N)_c/\partial\phi$ and stability boundary $(\lambda_N)_c$ with change of cutting edge setting angle θ ($n=3$, $\phi=0°$).

Fig. 67 shows the case of $\phi=-67.5°$, and in this setting condition $(\lambda_N)_{max}$ becomes maximum at four points as shown in Fig. 63. It is seen in the figure that $\partial(\lambda_N)_c/\partial g_1$, $\partial(\lambda_N)_c/\partial\phi>0$ near the first order and the second order of θ_{opt}. Considering that the value of $(\lambda_N)_{max}$ at the first order of θ_{opt} is slightly greater than that at the second order of θ_{opt}, and that the value of $\partial(\lambda_N)_c/\partial g_1$ at the first order

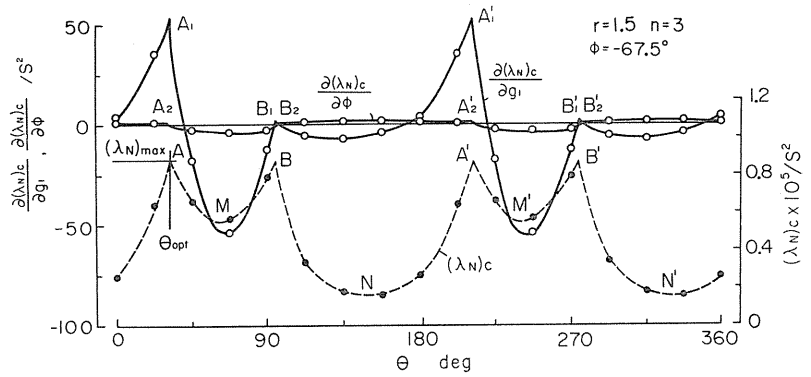

FIG. 67. Variation of differential coefficients $\partial(\lambda_N)_c/\partial g_1$, $\partial(\lambda_N)_c/\partial\phi$ and stability boundary $(\lambda_N)_c$ with change of cutting edge setting angle θ ($n=3$, $\phi=-67.5°$).

of θ_{opt} is fairly greater than that at the second order of θ_{opt}, the first order of θ_{opt} is favorable to the prevention of the chatter vibration.

4.2.2. Tools with four cutting edges ($n=4$)

4.2.2.1. Effect of ϕ

The stability boundary of the tools with four cutting edges which are set in a concyclic position as shown in Fig. 68. In this case, the values of g_i are determined by the next relations.

$$\left.\begin{aligned} g_1 &= 1+\phi/90 \\ g_2 &= g_3 = 1 \\ g_4 &= 1-\phi/90 \end{aligned}\right\} \qquad (53)$$

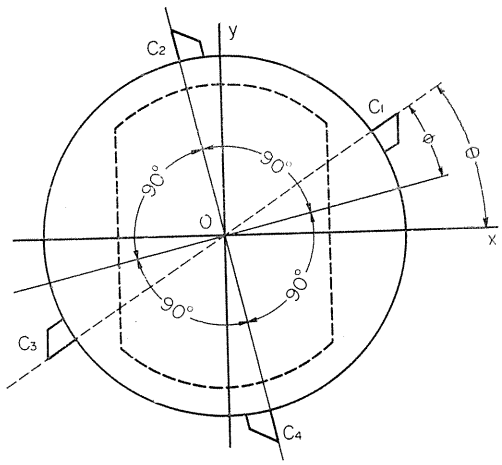

FIG. 68. Cutting edge setting angle ($n=4$).

Fig. 69 shows the result for the symmetrical setting condition ($\phi=0°$), Figs. 70~72 are the results for the case where two opposite cutting edges of four are shifted by the amount of ϕ.

It is seen in the figures that when $\phi=0°$, that is, in the symmetrical setting condition, the stability boundary $(\lambda_N)_c$ is not influenced by the cutting edge setting angle θ, and when $\phi=22.5°$, $\phi=45°$, $\phi=67.5°$, there exists the optimum cutting edge setting angle and the corresponding maximum value $(\lambda_N)_{max}$. Figs. 73, 74 show the relation between the maximum value $(\lambda_N)_{max}$, the corresponding optimum cutting edge setting angle θ_{opt} and the shifted angle ϕ. It is clear in these figures that in each tool system, the value of $(\lambda_N)_{max}$ becomes minimum when $\phi=0°$ (symmetrical setting condition), and in the tool systems which have the directional characteristics in the vibrational properties there is the optimum shifted angle ϕ_{opt} for the prevention of chatter vibration.

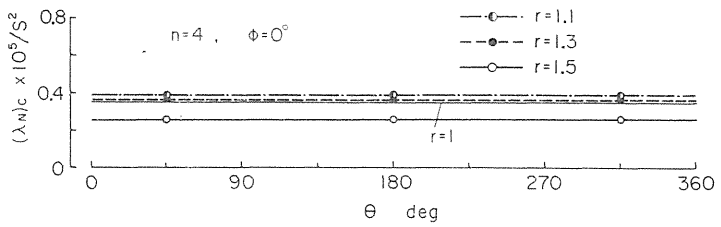

FIG. 69. Variation of stability boundary $(\lambda_N)_c$ with change of cutting edge setting angle θ ($\phi=0°$).

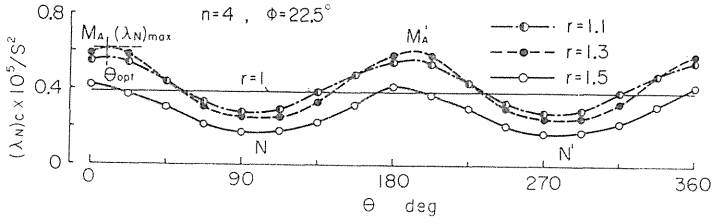

FIG. 70. Variation of stability boundary $(\lambda_N)_c$ with change of cutting edge setting angle θ ($\phi=22.5°$).

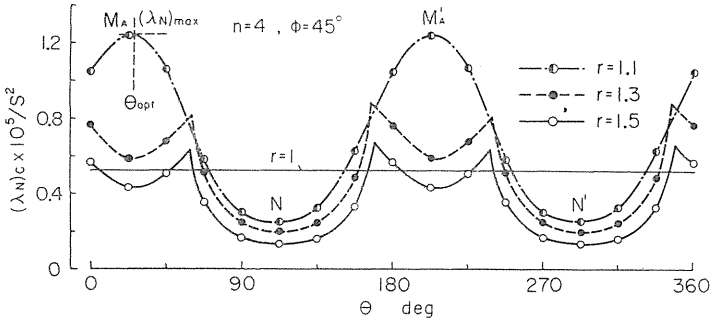

FIG. 71. Variation of stability boundary $(\lambda_N)_c$ with change of cutting edge setting angle θ ($\phi=45°$).

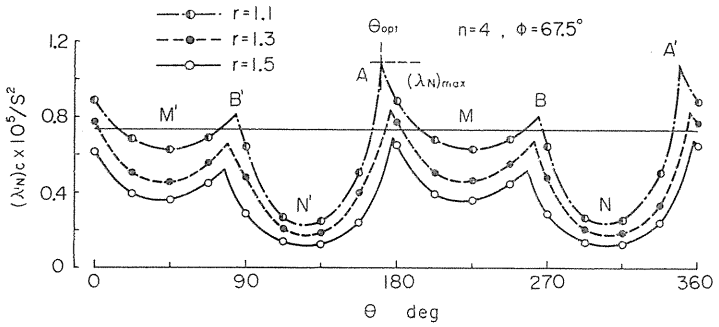

FIG. 72. Variation of stability boundary $(\lambda_N)_c$ with change of cutting edge setting angle θ ($\phi=67.5°$).

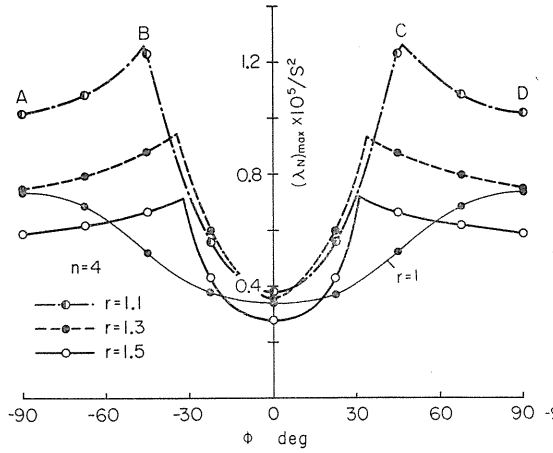

FIG. 73. Relation between maximum value $(\lambda_N)_{max}$ and shifted angle ϕ $(n=4)$.

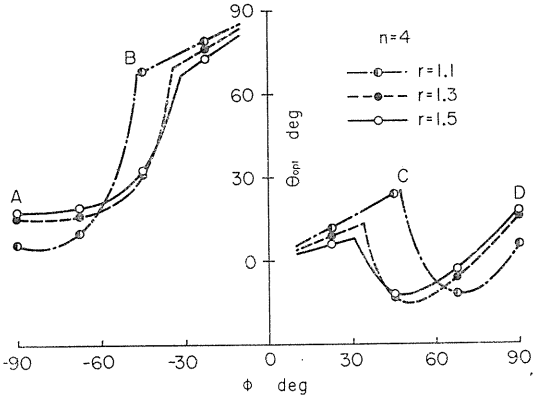

FIG. 74. Relation between optimum cutting edge setting angle θ_{opt} and shifted angle ϕ $(n=4)$.

4.2.2.2. Effect of small change in g, ϕ on stability boundary

In this section, the effect of a small change in g or ϕ on the stability boundary will be examined for the tools with four cutting edges.

Fig. 75 shows the variation of the differential coefficients $\partial(\lambda_N)_c/\partial g_1$, $\partial(\lambda_N)_c/\partial\phi$ with the change of the cutting edge setting angle θ for $\phi=0°$. A similar variational tendency to that in Fig. 66 $(n=3)$ can be observed in this figure. That is, though the stability boundary $(\lambda_N)_c$ is independent of the cutting edge setting angle θ in the case of $\phi=0°$, $(\lambda_N)_c$ is influenced by a small error in both g and ϕ. $\partial(\lambda_N)_c/\partial g_1>0$ at A, A' and $\partial(\lambda_N)_c/\partial\phi>0$ at D, D', so these cutting edge setting conditions are desiable to improve the chatter behaviour. From a practical point of view, however, the cutting edge setting angles θ_1, θ_2 are favorable, where both differential coefficients become positive simultaneously.

Next, Fig. 76 shows the result for $\phi=60°$ where the value of $(\lambda_N)_{max}$ becomes approximately maximum (See Fig. 73). It is recognized in the figure that the cutting edge setting angles (M_A, M_A') where the stability boundary $(\lambda_N)_c$ becomes

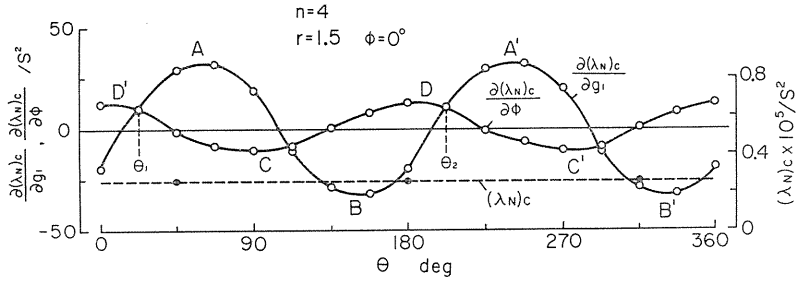

FIG. 75. Variation of differential coefficients $\partial(\lambda_N)_c/\partial g_1$, $\partial(\lambda_N)_c/\partial\phi$ and stability boundary $(\lambda_N)_c$ with change of cutting edge setting angle θ $(n=4, \phi=0°)$.

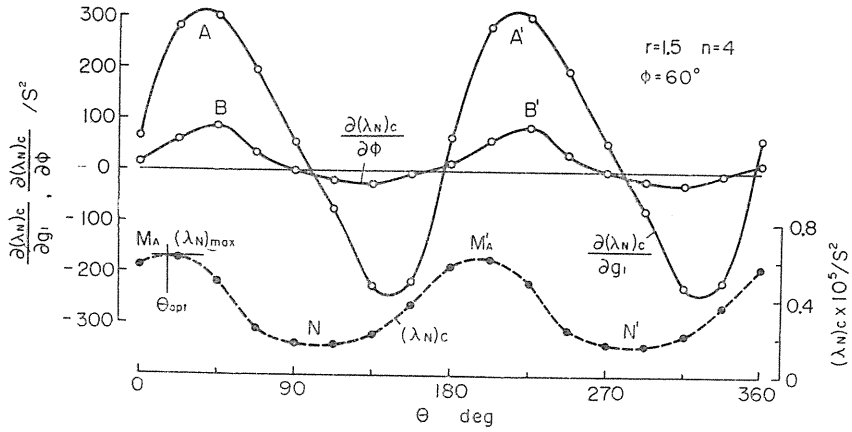

FIG. 76. Variation of differential coefficients $\partial(\lambda_N)_c/\partial g_1$, $\partial(\lambda_N)_c/\partial\phi$ and stability boundary $(\lambda_N)_c$ with change of cutting edge setting angle θ ($n=4$, $\phi=60°$).

maximum does not agree with the cutting edge setting angles where the differential coefficients become maximum, but $\partial(\lambda_N)_c/\partial g_1>0$, $\partial(\lambda_N)_c/\partial\phi>0$ at M_A, M'_A. Hence, from a practical point of view, these optimum cutting edge setting angles are favorable for the prevention of the chatter vibration.

4.2.3. Optimum tool configuration

From the above considerations, it is clear that the chatter behaviour is improved by the unsymmetrical setting condition ($\phi=0°$) for $n=3$, 4, too. As seen in Figs. 64, 73, however, the value of $(\lambda_N)_{max}$ is closely dependent on the frequency ratio r, hence, it is expected that there will be the optimum frequency ratio r_{opt} for the prevention of the chatter vibration.

Fig. 77 shows the relation between the maximum value $(\lambda_N)_{max}$ and the frequency ratio r for the various cutting edge setting conditions. It is seen in the figure that there is an optimum frequency ratio r_{opt}, namely, the optimum tool configuration for the prevention of the chatter vibration. This magnitude of r_{opt} is not affected by the number of the cutting edges and the setting conditions of each cutting edge, and is nearly agreeable with the optimum frequency ratio r_{opt}

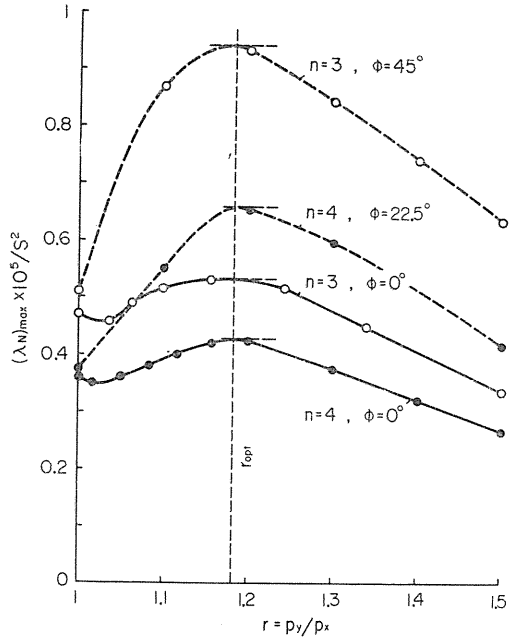

FIG. 77. Relation between maximum value $(\lambda_N)_{max}$ and frequency ratio r ($n=3$, 4).

for $n=2$ (See Fig. 27). This fact is considered favorable for the design of an effective multi-edge rotary cutting tool to prevent the chatter vibration.

4.3. Conclusion

The relation between the stability boundary of the multi-edge rotary cutting tool which has directional characteristics in the vibratinal properties and the various cutting edge setting conditions is examined from the practical point of view.

As a result, it has been shown that

(1) The chatter vibration can be prevented through a good use of the directional characteristics of the system and a proper combination of the setting angles of each cutting edge, in the multi-edge rotary cutting tool with 2, 3 or 4 cutting edges; and

(2) There is an optimum tool configuration to prevent the chatter vibration, and this configuration is not affected by the number of the cutting edges and the setting angles of each cutting edge.

Furthermore, the effect of a small error in the tool setting condition and the tool dimensions (such as cutting angle, nose radius etc.) is studied for many practical cases.

Acknowledgement

The authors wish to thank the members of the Laboratory of Mechanical Technology, Nagoya University, who assisted in the research work.

Reference

1) R. S. Hahn: Trans. ASME., **75** (1953), 1073; Trans. ASME., **76** (1954), 593.
2) S. A. Tobias: Trans. ASME., **80** (1958), 1079; "Machine-tool vibration", (1965), Blackie; J. P. Gurney and S. A. Tobias: Int. J. Mach. Tool Des. Res., **1** (1961), 325; Trans. ASME., **84** (1962), 103;
G. Sweeney and S. A. Tobias: Proceedings International Research in Production Engineering, Pittsburgh (1963), 475, ASME.
3) J. Tlusty and M. Polacek: Proceedings International Research in Production Engineering, Pittsburgh (1963), 465, ASME; "Selbsterregte Schwingungen an Werkzeugmaschinen", (1963), Verlag Technik, Berlin.
4) S. Doi and S. Kato: Trans. Japan Soc. Mech. Engrs., **19** (1953), 28; Trans. Japan Soc. Mech. Engrs., **20** (1954), 61; Trans. Japan Soc. Mech. Engrs., **21** (1955), 727; Trans. Japan Soc. Mech. Engrs., **22** (1956), 408; Trans. ASME., **78** (1956), 1127.
S. Kato: Trans. Japan Soc. Mech. Engrs., **21** (1955), 110; Trans. Japan Soc. Mech. Engrs., **24** (1958), 115.
5) H. E. Merrit: Trans. ASME., Series B, **87** (1965), 447;
G. W. Long and J. R. Lemon: Trans. ASME., Series B, **87** (1965), 455; Machine Tool Design and Research (1964), 545, Pergamon Press;
R. L. Kegg: Trans. ASME., Series B, **87** (1965), 464;
J. R. Lemon and P. C. Ackermann: Trans. ASME., Series B, **87** (1965), 471;
R. Sridhar *et al.*: Trans. ASME., Series B, **90** (1968), 317; Trans. ASME., Series B, **90** (1968), 325; Trans. ASME., Series B, **90** (1968), 330.
6) R. S. Hahn: Trans. ASME., **73** (1951), 331.
7) S. Kato *et al.*: Trans. Japan Soc. Mech. Engrs., **21** (1955), 727.
8) K. L. Kuchma: The Engineers Digest, **18** (1957), 68.

9) S. Kato and E. Marui: Trans. Japan Soc. Mech. Engrs., **33** (1967), 1685.
10) S. Kato *et al.*: ASME Preprint, 68-WA/Prod-1.
11) S. Kato *et al.*: Trans. Japan Soc. Mech. Engrs., **34** (1968), 1610; Bulletin of JSME, **12** (1969), 584.
12) S. Kato and E. Marui: Trans. Japan Soc. Mech. Engrs., **34** (1968), 1619; Bulletin of JSME, **12** (1969), 593.
13) S. Kato and E. Marui: J. Japan Soc. Precision Engr., **35** (1969), 15.